Naval Research Laboratory

Washington, DC 20375-5320

NRL/MR/6180--97-7908

Upward Flame Spread on Vertical Surfaces

F.W. WILLIAMS

Navy Technology for Safety and Survivability
Chemistry Division

C.L. BEYLER
S.P. HUNT
N. IQBAL

Hughes Associates, Inc.
Baltimore, MD

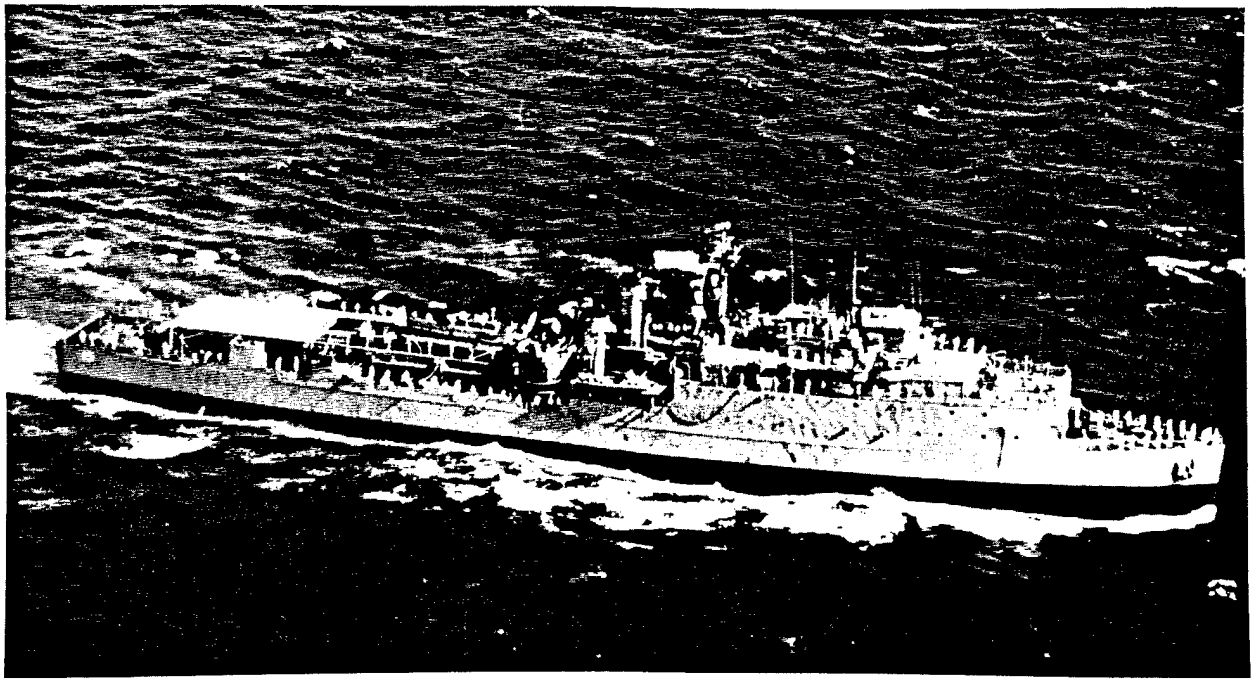

January 13, 1997

DTIC QUALITY INSPECTED 3

Approved for public release; distribution unlimited.

19970130 079

REPORT DOCUMENTATION PAGE

Form Approved
OMB No. 0704-0188

Public reporting burden for this collection of information is estimated to average 1 hour per response, including the time for reviewing instructions, searching existing data sources, gathering and maintaining the data needed, and completing and reviewing the collection of information. Send comments regarding this burden estimate or any other aspect of this collection of information, including suggestions for reducing this burden, to Washington Headquarters Services, Directorate for Information Operations and Reports, 1215 Jefferson Davis Highway, Suite 1204, Arlington, VA 22202-4302, and to the Office of Management and Budget. Paperwork Reduction Project (0704-0188), Washington, DC 20503.

1. AGENCY USE ONLY (*Leave Blank*)	2. REPORT DATE	3. REPORT TYPE AND DATES COVERED
	January 13, 1997	March 1995 — March 1996/Interim Report

4. TITLE AND SUBTITLE

Upward Flame Spread on Vertical Surfaces

5. FUNDING NUMBERS

PE — 63514N
PS — 1565

6. AUTHOR(S)

F.W. Williams, C.L. Beyler,* S.P. Hunt,* and N. Iqbal*

7. PERFORMING ORGANIZATION NAME(S) AND ADDRESS(ES)

Naval Research Laboratory
Washington, DC 20375-5320

8. PERFORMING ORGANIZATION REPORT NUMBER

NRL/MR/6180--97-7908

9. SPONSORING/MONITORING AGENCY NAME(S) AND ADDRESS(ES)

Chief of Naval Operations (N86D)
Washington, DC 20350

Naval Sea Systems Command (Code 03R2)
2531 Jefferson Davis HW
Arlington, VA 22242-5160

10. SPONSORING/MONITORING AGENCY REPORT NUMBER

11. SUPPLEMENTARY NOTES

*Hughes Associates, Inc., Baltimore, MD

12a. DISTRIBUTION/AVAILABILITY STATEMENT

Approved for public release; distribution unlimited.

12b. DISTRIBUTION CODE

13. ABSTRACT (*Maximum 200 words*)

A model which describes the physical processes of upward flame spread and fir growth on wall materials has been developed and implemented as a computer program. The computer based flame spread model simulates the fire growth along a vertical combustible wall. The vertical wall material may be heated by an imposed external heat flux and is ignited at its bottom edge with a flame from a line burner of user specified strength. The model predicts theflame spread rate, the heat release rate of the fire, the flame height, the net heat flux to the wall surface and the time varying surface temperatures. The model uses inputs developed from cone calorimeter data. The results from the model compare favorably to experimental upward flame spread results for polymethylmethacrylate, plywood and wood particle board found in the literature. The sensitivity of the model to material thermal properties, flame heat flux and flame height are systematically examined.

14. SUBJECT TERMS

Vertical flame spread
Computer program
Validations
Wall fire
Predictions
Material properties
Small and real-scale fire tests

15. NUMBER OF PAGES

71

16. PRICE CODE

17. SECURITY CLASSIFICATION OF REPORT	18. SECURITY CLASSIFICATION OF THIS PAGE	19. SECURITY CLASSIFICATION OF ABSTRACT	20. LIMITATION OF ABSTRACT
UNCLASSIFIED	UNCLASSIFIED	UNCLASSIFIED	SAR

NSN 7540-01-280-5500

Standard Form 298 (Rev. 2-89)
Prescribed by ANSI Std 239-18
298-102

CONTENTS

FIGURES

FIGURES (Continued)

TABLES

Upward Flame Spread on Vertical Surfaces

1.0 INTRODUCTION

In this report, a vertical flame spread model is developed and validated against literature data. This work is a part of the U.S. Navy Materials Test program and is designed to provide a technique for specifying the performance required for the U.S. Navy material applications in terms of small-scale tests. This program will result in known fire performance of material applications and will allow manufacturers/developers to provide cost-effective materials with the required performance, leading to cost saving and known performance.

The upward flame spread model on vertical surfaces is part of the modeling effort designed to develop a general modeling framework which will assess performance of materials in Navy fire scenarios from small-scale test data. This model is formulated on the basis of a review of the fire dynamics literature relevant to fire growth presented by Williams and Beyler, 1994 (reference (1)).

2.0 THEORY AND DESCRIPTION OF THE MODEL

A computer model has been developed which calculates the flame spread on a vertical wall subjected to a line ignition source. Flame spread is calculated using sub-models derived from the literature utilizing inputs determined from cone calorimeter tests (reference (2)). The model is formulated based on existing sub-models for (1) ignition, (2) material heating, pyrolysis, and burning rate, (3) flame spread, and (4) flame and surface heat transfer. The details for each component of the analysis will be described in the following sections.

2.1 Model Summary

The computer model calculates the flame spread on a vertical surface by breaking up the surface into a large number of elements. The conditions of each element are independently computed. The centroid of an element is assumed to be representative of the entire element (Fig. 1). There are a number of global conditions that are calculated by summing the contributions from each element: the heat release rate, the height of the pyrolysis region, the flame height above the base of the wall, and the height of burnout front above the base of the wall.

Each element is in one of four states: (1) preheat (above the flame), (2) preheat (exposed to the flame), (3) burning, and (4) consumed. The model keeps track of these conditions for each element, and the model stops when either the user entered simulation time is reached, the fuel is entirely consumed, or the flame propagation ceases.

Manuscript approved December 4, 1996.

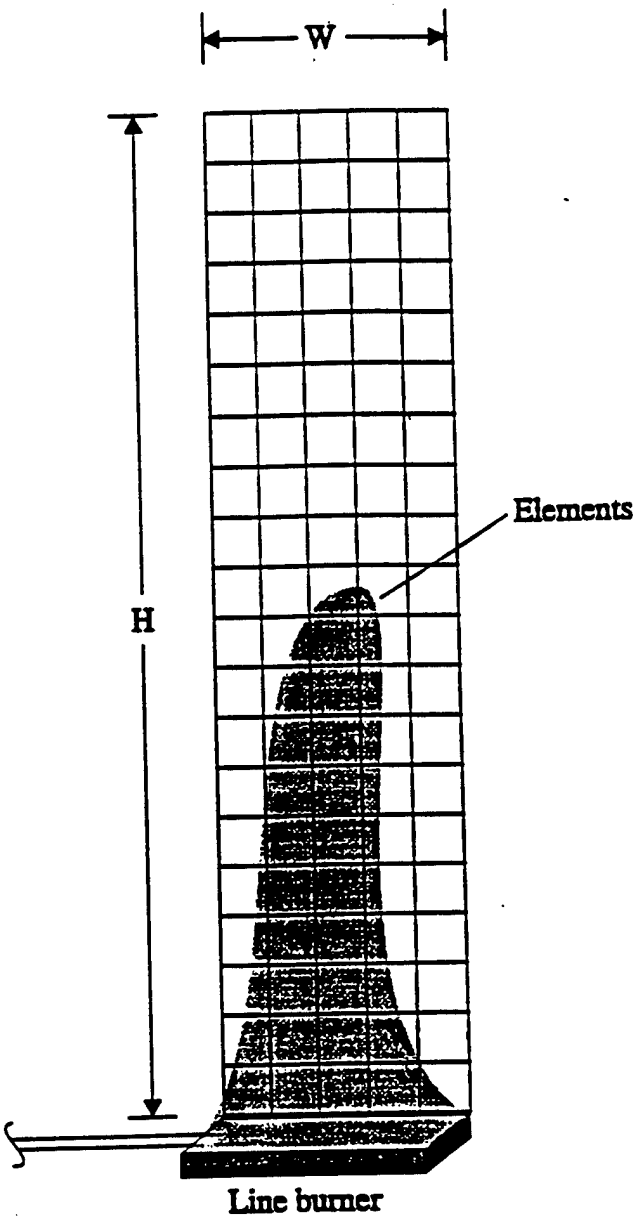

Figure 1 Line fire configuration against the wall

2.2 Wall Flame Heights and Heat Fluxes to the Surface

In the present model, the wall can be heated by three sources: (1) an imposed external heat flux, (2) a line fire placed against the base of the wall (the ignitor), and (3) the wall flame itself. It has been shown that the heat flux to the wall from line fires against the wall and the wall itself can be correlated in the same manner.

Fig. 2 shows a correlation of the heat flux from a methane line burner to an adjacent wall along with similar results for fires involving liquid fuels saturated on the lower portion of a wall. This correlation can be expressed as follows:

$$\dot{q}'' = 20 \frac{kW}{m^2} \qquad \frac{y}{y_f} < 0.34$$

$$\dot{q}'' = 6.23\, y^{-1.07} \frac{kW}{m^2} \qquad 0.34 \le \frac{y}{y_f} < 0.7$$

$$\dot{q}'' = 3.59\, y^{-2.32} \frac{kW}{m^2} \qquad \frac{y}{y_f} > 0.7 \qquad (1)$$

where $\dot{q}''$ is the incident heat flux from the line burner to the wall surface (kW/m^2),
y is the height above the base of the wall (m), and
y_f is the flame height above the base of the wall (m).

This correlation is useful for representing methane burner ignitor and commonly used liquid ignitor fuels.

An alternative approach available in the model is the use of one of the wall fire heat flux correlations listed later in this section. These correlations are based on more luminous fuels which are typical of wall flames and non-methane line burners. The result of using the wall heat flux correlations is a more rapid ignition; however, the fire growth will be similar.

Equation (1) requires the determination of the flame height. There are several flame height correlations available for a line fire against a wall or wall fires (references (4) and (5)). Each of these takes the form:

$$y_f = C_f \dot{Q}'^{\frac{2}{3}} \qquad for \quad \frac{y_f}{y_p} > R$$

$$y_f = R y_p \qquad for \quad \frac{C_f \dot{Q}'^{\frac{2}{3}}}{y_p} < R \qquad (2)$$

where y_f is the wall flame height (m),
y_p is the pyrolysis height (m),
$\dot{Q}'$ is the heat release rate per unit length of the line burner (kW/m),
C_f is a constant ($m^{5/3}/kW^{2/3}$), and
R is the minimum ratio of the flame height to the pyrolysis height.

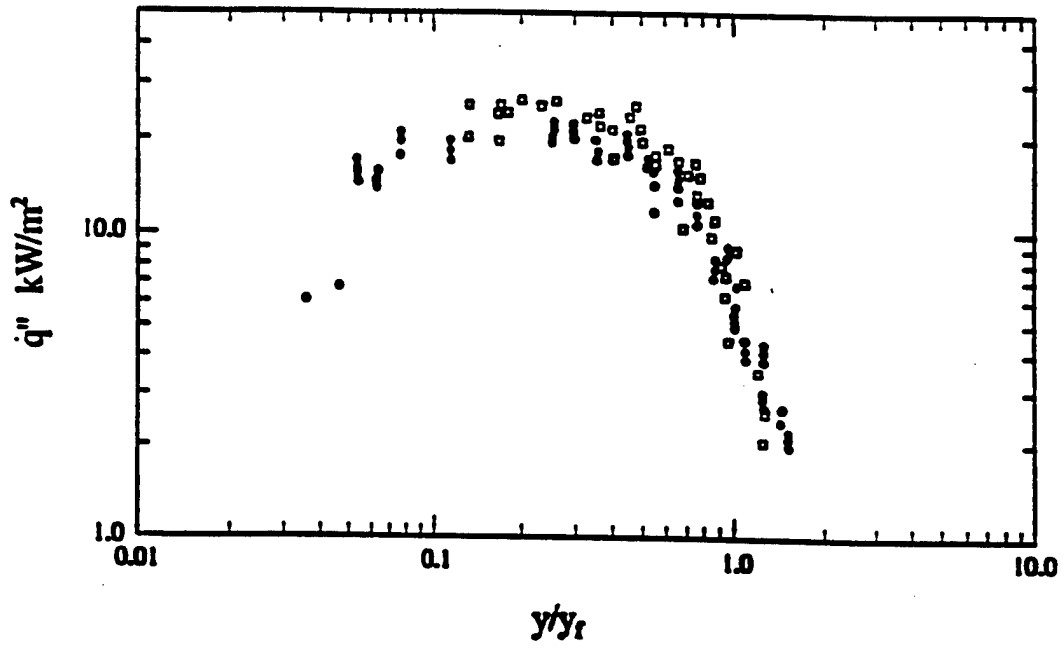

Fig. 2 - Wall heat flux distribution due to wall fires. The solid symbols are for a methane line burner fire adjacent to a wall and the open symbols are for liquid saturated wall fires with low flame intensity (reference (3))

Delichatsios (reference (4)) recommends $C_f = 0.052\ m^{5/3}/kW^{2/3}$, and Tu and Quintiere (reference (5)) recommend $C_f = 0.0666\ m^{5/3}/kW^{2/3}$. The second part of Equation (2) is applicable to wall fires with low heat release rates per unit area where the first part of Equation (2) would erroneously indicate that the flame height is less than the pyrolysis height. Based on work by Tewarson (reference (6)), R, the minimum ratio of the flame height to the pyrolysis height, is in the range of 1.0-1.1. One of the goals of the comparison with experimental data is to determine which value of C_f from the literature is most appropriate for use in vertical flame spread predictions.

Upon the ignition of the wall, the luminosity of the flame may increase over that typical of the methane ignitor flame. To compensate for this, the model allows the use of a different heat flux correlation after ignition of the wall. The incident heat flux from wall flames to the surface has been experimentally determined for a number of materials. Fig. 3 shows wall heat flux distributions from wall flames to the adjacent wall. The outline in Fig. 3 encloses most of the steady state heat flux data available as summarized by Quintiere (reference (7)). Based on Fig. 3, three different curve fits have been developed as shown in Fig. 3a for line diffusion flames to a vertical wall. Mitler (reference (8)) also calculated heat fluxes from the wall flames back to the wall ignited by a flame from a 10 kW/m line burner and compared with the data of Quintiere (reference (7)).

An upper bound fit to Fig. 3,

$$\dot{q}''_e = 12.7\left(\frac{(y-y_b)}{(y_f-y_b)}\right)^{-2.41} \qquad \frac{(y-y_b)}{(y_f-y_b)} \geq 0.7 \tag{3}$$

$$\dot{q}''_e = 30\ \frac{kW}{m^2} \qquad \frac{(y-y_b)}{(y_f-y_b)} < 0.7 \tag{4}$$

a lower bound fit to Fig. 3,

$$\dot{q}''_e = 2.71\left(\frac{(y-y_b)}{(y_f-y_b)}\right)^{-2.21} \qquad \frac{(y-y_b)}{(y_f-y_b)} \geq 0.43 \tag{5}$$

$$\dot{q}''_e = 18\ \frac{kW}{m^2} \qquad \frac{(y-y_b)}{(y_f-y_b)} < 0.43 \tag{6}$$

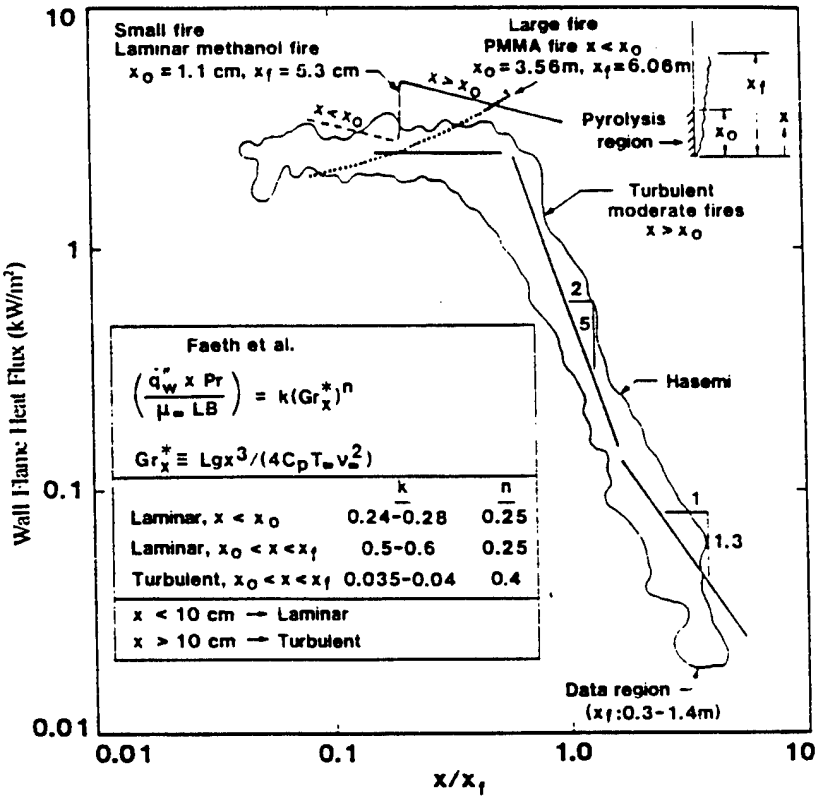

Figure 3 Flame heat flux distribution for wall fires in terms of y/y_f. (reference (7))

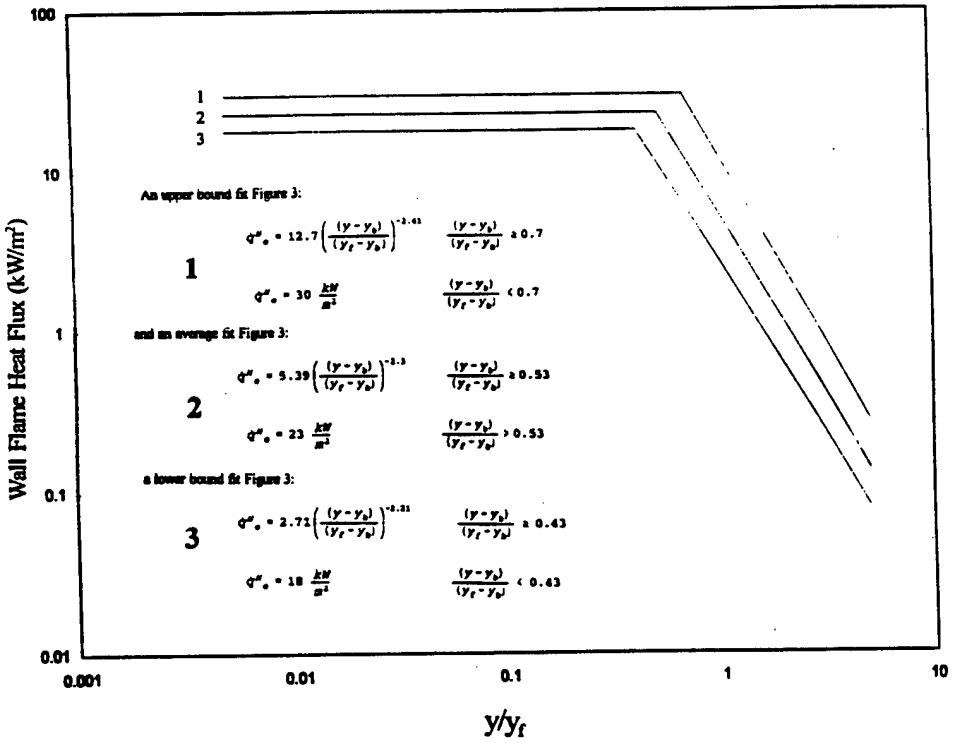

Figure 3a Wall flame heat flux correlations (reference (8))

and an average fit to Fig. 3:

$$\dot{q}''_e = 5.39\left(\frac{(y-y_b)}{(y_f-y_b)}\right)^{-2.3} \qquad \frac{(y-y_b)}{(y_f-y_b)} \geq 0.53 \tag{7}$$

$$\dot{q}''_e = 23\ \frac{kW}{m^2} \qquad \frac{(y-y_b)}{(y_f-y_b)} < 0.53 \tag{8}$$

where y is the height above the base of the burning wall (m),
y_b is the height of the burnout front (m), and
y_f is the height of the flame tip above the base of the burning wall.

Under spreading conditions with burnout occurring, the y_f should be replaced by $y_f - y_b$

The selection among these correlations will depend on the flame luminosity and the level of conservatism required. As the various heat flux correlations available span a considerable range of incident heat fluxes, one of the goals of the comparison with experimental data is to determine which of these correlations from the literature is most appropriate for use in vertical flame spread predictions.

2.3 Surface Heating and Ignition

Prior to ignition, the wall surface is assumed to be a semi-infinite one-dimensional slab with a time dependent surface heat flux determined from the wall flame and external sources as described in Section 2.2. The conduction model used in this computer model is an approximate solution to the semi-infinite slab problem using an assumed cubic temperature profile and an integral solution (reference (9)). This method was selected based on its excellent predictive performance and computational efficiency.

The temperature profile within the wall is assumed to be approximated by the following equation (refer Fig. 4):

$$T(z) = \overline{A}z^3 + \overline{B}z^2 + \overline{C}z + \overline{D} \tag{9}$$

where z is the distance from the surface and
the constants A, B, C, and D may be determined from the boundary conditions:

$$at\ z = \delta, \qquad T = T_o \tag{9a}$$

$$at\ z = \delta, \qquad \frac{\partial T}{\partial z} = 0 \tag{9b}$$

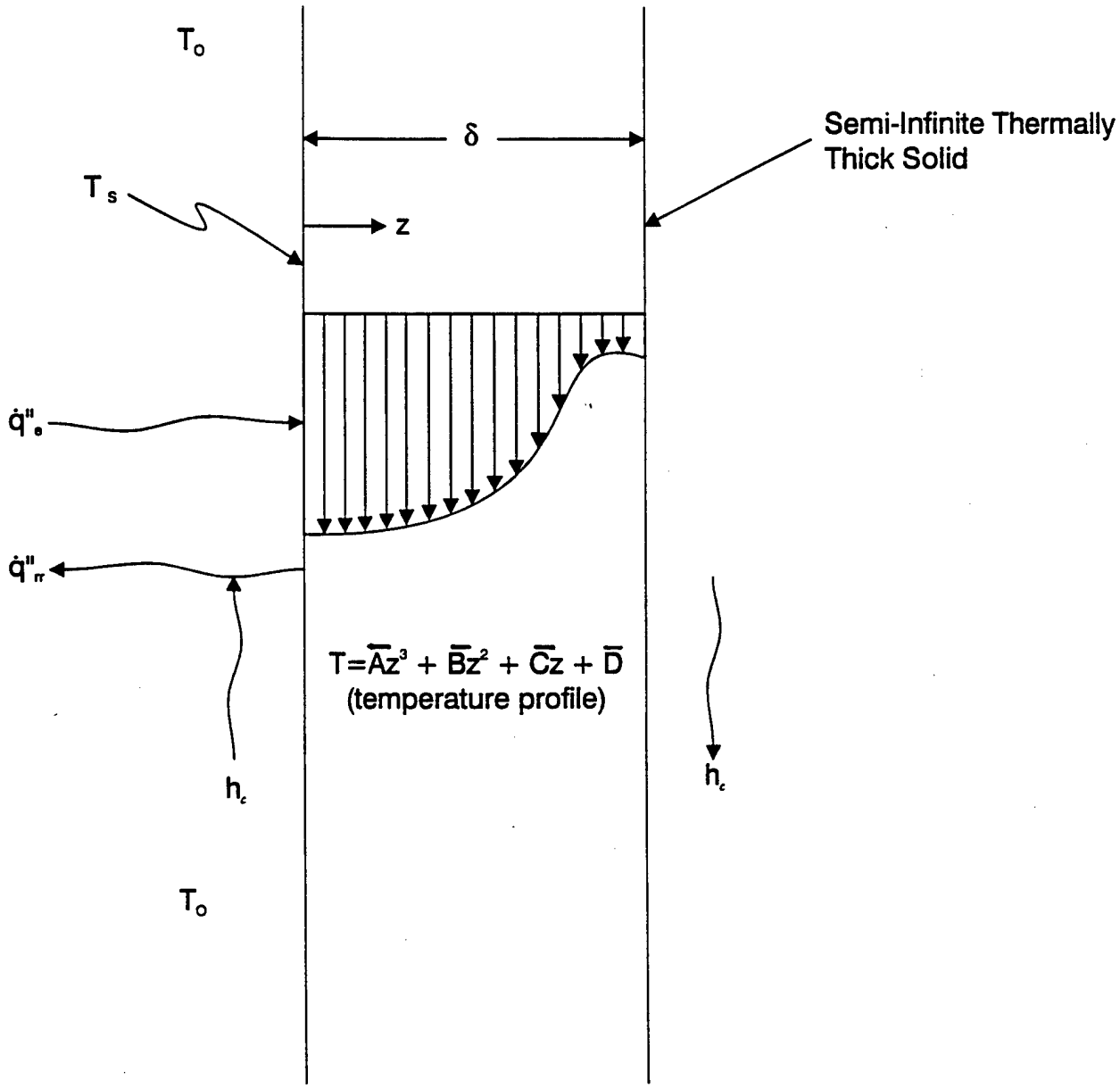

Figure 4 Temperature distribution in the solid during preheating

$$at\ z = 0 \qquad -k\frac{\partial T}{\partial z} = \dot{q}''_{net} \tag{9d}$$

The resulting temperature profile becomes

$$T_s = T_o + \frac{\dot{q}''_{net}\delta}{3k}\left[1-\frac{z}{\delta}\right]^3 \tag{10}$$

where T_o is the initial surface temperature (°C or K),
δ is the thermal penetration depth (m),
z is the depth into the wall surface (m), and
k is the thermal conductivity (kW/m-K).

This profile may be inserted into an integral form of the energy equation:

$$\frac{d}{dt}\int_0^{\delta}(T-T_o)\,dy = -\alpha\left(\frac{\partial T}{\partial z}\right) \tag{11}$$

where α is the thermal diffusivity (m^2/sec). The surface temperature at any time is then given by the following differential equation:

$$\frac{d}{dt}\left(\frac{T_s(t)-T_o}{\dot{q}''_{net}}\right)^2 = \frac{4\ \dot{q}''_{net}}{3\ k\rho c} \tag{12}$$

where ρ is the density (kg/m^3) and c is the thermal heat capacity (kJ/kg-K). The net heat flux as a function of the wall surface temperature is:

$$\dot{q}''_{net} = \dot{q}''_{e} + \dot{q}''_{imp} - \sigma\epsilon[T_s(t)^4 - T_o^4] - h_c[T_s(t) - T_o] \tag{13}$$

where $\dot{q}''_e$ is the incident heat flux from the flame to the surface (kW/m^2),
$\dot{q}''_{imp}$ is the externally imposed radiant heat flux (kW/m^2),
h_c is the heat transfer coefficient (kW/m^2-K)),
T_s is the surface temperature (°C or K), and
T_o is the ambient temperature (°C or K).

The convective loss term is used only during radiative preheating prior to flame initiation where flame/plume convective heating is absent. Carrying out the differentiation of Equation (12) and differentiating Equation (13) with respect to time yields a differential equation with $T_s(t)$ as the only unknown term:

$$2\ (T_s(t) - T_o)\frac{dT_s(t)}{dt} - \frac{[T_s(t) - T_o]^2}{\dot{q}''_{net}(t)}\frac{d\dot{q}''_{net}(t)}{dt} = \frac{4\ \dot{q}''_{net}}{3\ k\rho c} \qquad (14)$$

$$\frac{d\dot{q}''_{net}(t)}{dt} = -\ 4\ T_s(t)^3\frac{d\dot{q}''_{net}(t)^3}{dt} \qquad (15)$$

Equations (14) and (15) are solved in the flame spread model using a fourth order Runge-Kutta method for each time step. This provides a very efficient method for predicting the heating of the surface up to the ignition temperature. The thermal inertia, kpc, is determined from ignition experiments in the cone calorimeter.

In the early stages of the temperature rise, the differential equations do not converge due to a singularity when T_s (t) is equal to T_o. For small temperature rises Equation (16), a lower order method without this singularity, was employed to determine the temperature rise of the surface. This method uses an average net surface heat flux and is a single calculation from the initial temperature:

$$T_s = T_\infty + 2\overline{\dot{q}''_{net}}(t)\sqrt{\frac{t}{\pi\ (k\rho c)}} \qquad (16)$$

where $\dot{q}''_{net}$ is the average net heat flux received at the surface (kW/m^2) over time t (sec). It was determined that Equations (14) and (15) have convergence problems up to a surface-initial temperature rise no greater than 2-3 K and that both methods were in fair agreement up to a temperature rise of 50-100 K. Equation (16) is used in the model for only one or two time steps. The material properties, the heat flux level, and the duration of the heat flux levels all determine where the integral method begins to converge.

2.4 Heat Release Rate

Once an element has reached the ignition temperature, it is allowed to pyrolyze, burn and contribute energy to the wall fire. The heat release rate of the wall is determined by summing up the heat release rates of each burning element:

$$\dot{Q} = \Delta H_c \sum_{i=1}^{n} \dot{m}''(x, y, z, t)\ A\ (x, y) \qquad (17)$$

where n is the number of elements which are burning at time t (sec),
ΔH_c is the heat of combustion of the wall material (kJ/kg),
$\dot{m}''(x, y, z, t)$ is the spatially and temporally varying mass loss rate per unit area (kg/m^2), and
A(x, y) is the area of the element under consideration (m^2).

Both elemental area and the mass loss rate are allowed to vary from element to element, although there is currently no convenient way to specify elements of variable size implemented in the current model, i.e., adaptive gridding. The mass loss rate for each element is given by

$$\dot{m}''(t) = \frac{\dot{q}''_{net}(t)}{\Delta h_g(t)} \tag{18}$$

where Δh_g is the heat of gasification (kJ/kg) as determined from the cone calorimeter. The net energy ($\dot{q}''_{net}$) absorbed by each burning element can be calculated from the following equation:

$$\dot{q}''_{net} = \dot{q}''_{imp} + \dot{q}''_{e} - \sigma\epsilon\,[T_s(t)^4 - T_o^4] \tag{19}$$

where $\dot{q}''_{imp}$ is the radiant imposed heat flux,

T_s is the surface pyrolysis temperature (°C or K),
T_o is the ambient temperature (°C or K),
σ is the Stefan-Boltzman constant (5.668E-08 W/m^2-K^4), and
ϵ is the surface emissivity.

2.5 Material Property Data

The material properties required by the model are determined using the cone calorimeter ASTM standard test method E-1354 (reference (2)). These properties are as follows:

1. Ignition temperature, T_{ig}, (K);
2. Thermal inertia, kρc, (kW/m^2-K)^2 sec;
3. Effective heat of gasification, Δh_g, (kJ/kg); and
4. Heat of combustion, ΔH_c, (kJ/kg).

The ignition temperature may be measured directly in the cone calorimeter test or it may be estimated. If the value is estimated, a set of ignition temperature-thermal inertia values will result and additional information is necessary in order to determine the most appropriate pair. The thermal inertia is determined by trial and error as follows:

The ignition times for a series of heat fluxes is first obtained from the cone for the material in question. The flame spread model is then used to predict the ignition time for the given ignition temperature, applied radiant flux and thermal inertia. By holding the ignition temperature constant and altering the thermal inertia such that the ignition times are predicted for each applied radiant flux, a thermal inertia is established for the ignition temperature. Figures 5 and 6 show the actual and predicted ignition times for various flux levels at two assumed ignition temperatures, 317°C and 350°C.

The effective heat of gasification is derived from the cone calorimeter mass loss rate measurements (Fig. 7). The heat of gasification varies with time, but an average value may be used. Use of heat of gasification that varies substantially from instant to instant (as is often the case in cone measured data) would produce heat release rate and flame height predictions with oscillations of similar intensity. The heat of gasification is estimated from the following equation:

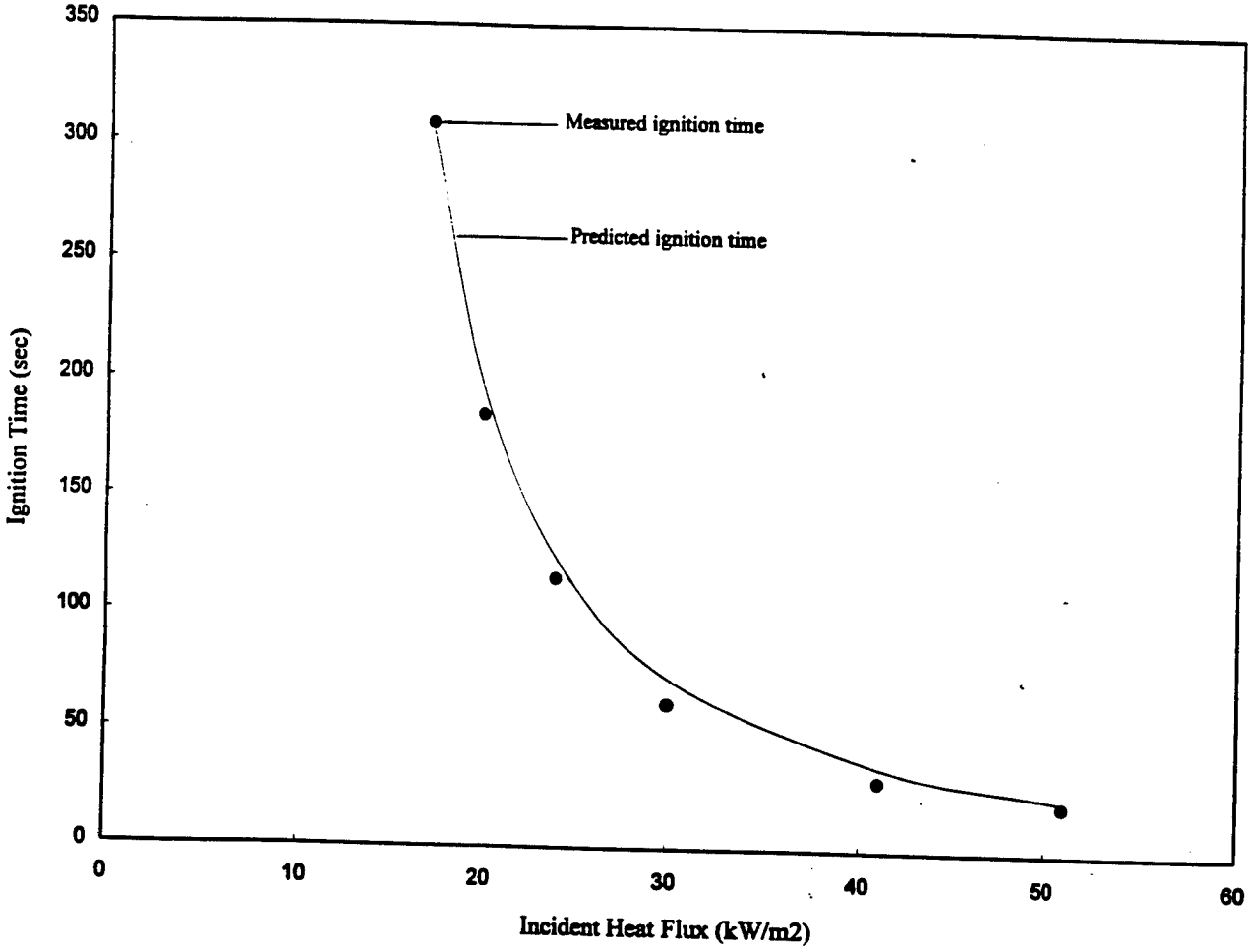

Figure 5 Comparison of experimental and predicted ignition time for plywood at T_{ig} = 317 °C, and $k\rho c$ = 0.73 (kW/m^2 K)^2 sec. Data from Quintiere and Harkleroad, 1985 (reference (10))

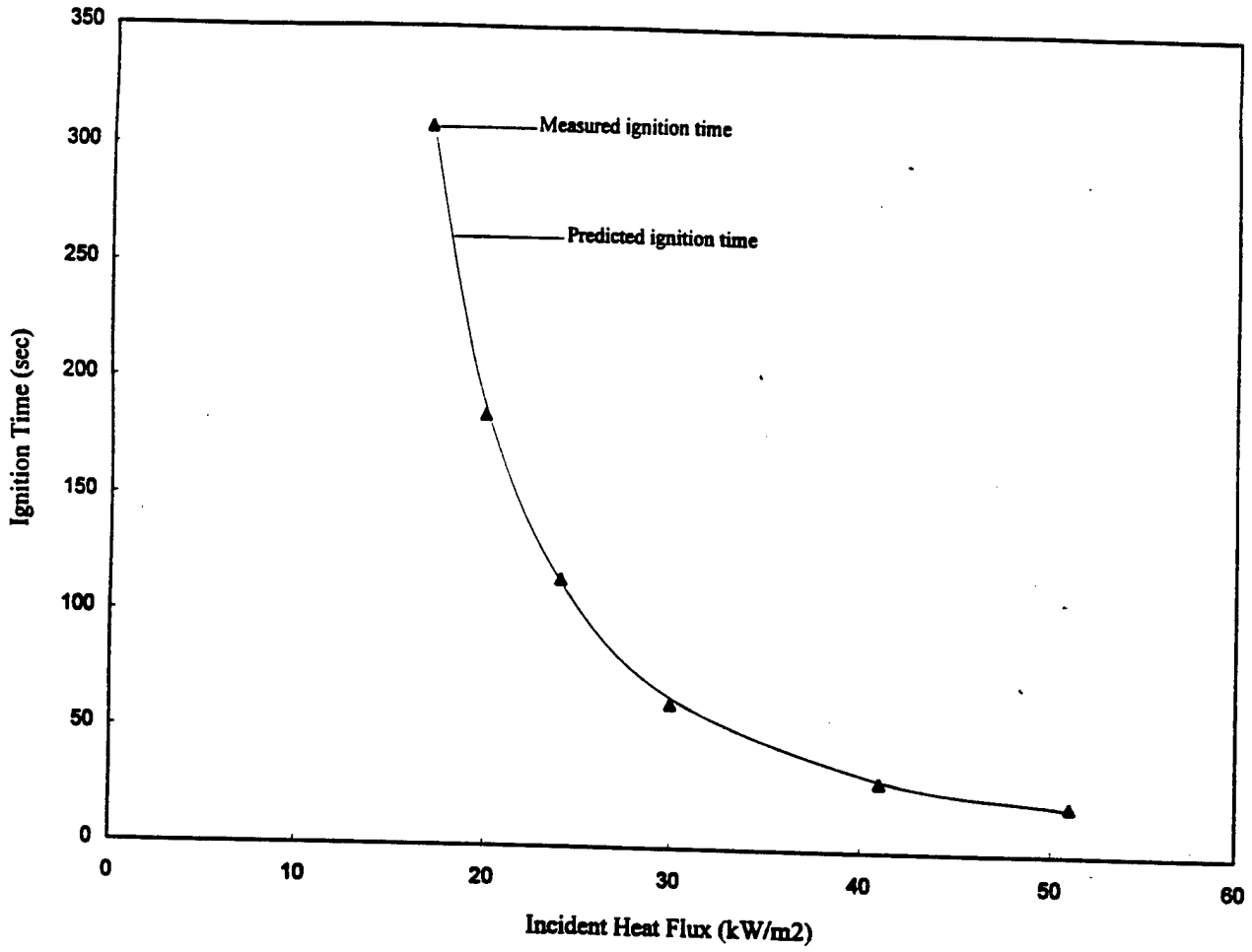

Figure 6 Comparison of experimental and predicted ignition time for plywood at T_{ig} = 350 °C, and $k\rho c$ = 0.475 $(kW/m^2\ K)^2$ sec. Data from Quintiere and Harkleroad, 1985 (reference (10))

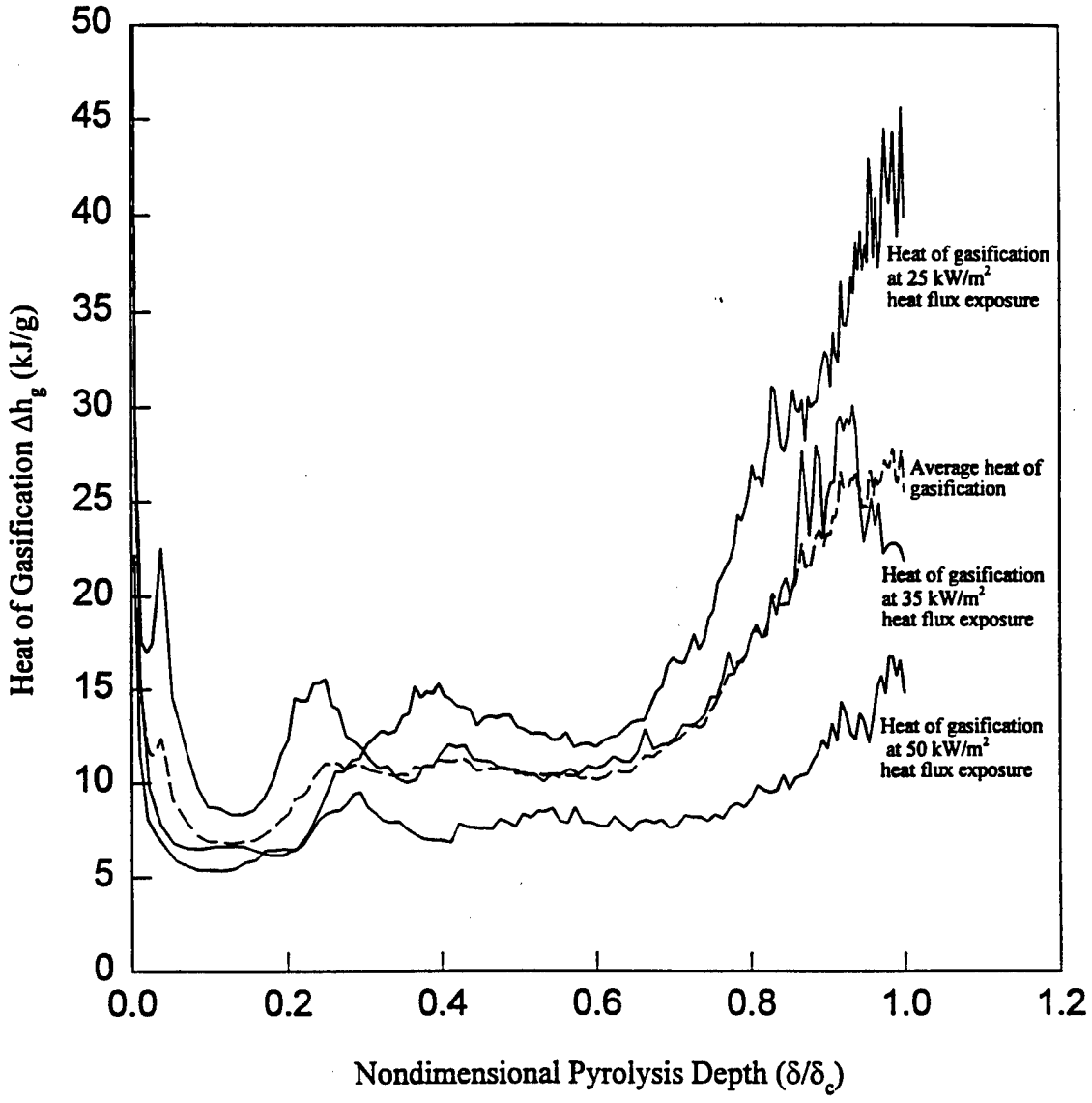

Figure 7 Cone Calorimeter heat of gasification for cardboard at various heat flux exposure

$$\Delta h_g(t) = \frac{\dot{q}''_{net}(t)}{\dot{m}''(t)} \tag{20}$$

where $\dot{q}''_{net}$ is the net heat flux per unit area incident on the surface of the material and $\dot{m}''$ is the mass loss rate per unit area. The net heat flux is the summation of the imposed radiant flux, the radiative and convective flux from the flame to the surface and the radiant heat loss from the surface to the surroundings. These terms are listed in Equation 19 of the previous section. In order to generalize the heat of gasification values for variable heat flux levels, the time dependent heat of gasification is transformed to a thickness dependent heat of gasification by replacing time with the pyrolysis penetration depth at that time (δ):

$$\Delta h_g(\delta) = \Delta h_g\,[(\delta(t)] = \Delta h_g(t) \tag{21}$$

where $\delta(t)$ is the nondimensional pyrolysis depth at time t and is determined from

$$\delta(t) = \frac{\sum_{i=1}^{n} \dot{m}_i''\,\Delta t_i A - m_f}{m_i - m_f} \tag{22}$$

where Δt_i is the time interval of the mass loss rate measurement (s), A is the specimen surface area (m^2), m_f is the final specimen mass (kg), and m_i is the initial specimen mass (kg).

The effective heat of combustion $\Delta H_{c,eff}$ is calculated in accordance to the methods given in ASTM E 1354 (reference (2)). This is given as:

$$\Delta H_{c,\,eff} = \frac{\sum_{i=1}^{n} \dot{q}_i \Delta t_i}{m_i - m_f} \tag{23}$$

where $\dot{q}_i$ is the heat release rate at time i as determined by the test.

3.0 PROGRAM DESCRIPTION

The upward flame spread program is written in LAHEY FORTRAN 90, and the following is a detailed description of the main program and the major subroutines.

There are subroutines for reading data, calculating results, and reporting the results to a file or printer. The main program calls the subprograms or subroutines that read the data and calculates the surface temperature at each element/node, heat release rate, and flame height. The subroutines structure of the model is illustrated in the flow chart of Fig. 8.

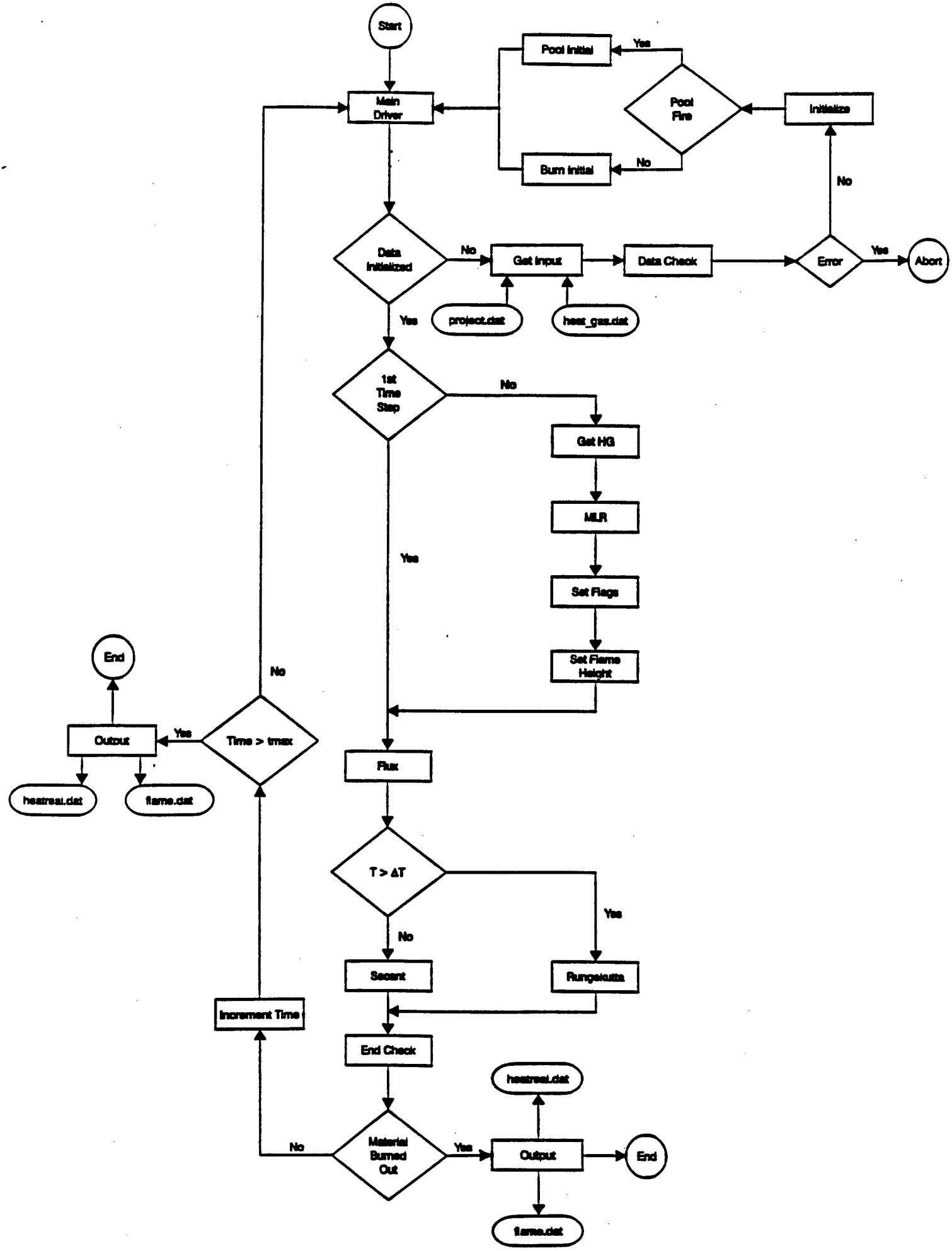

Figure 8 Flow chart for main program logic

3.1 Sub-models in the Numerical Simulation Computer Program

The program structure is divided into a main driver responsible for calling the various subroutines in the required order: *Initialization subroutines* that are used only once, the *calculation and updating subroutines* and *functions*, and the *output* and *termination subroutines*. The main driver calls three ***initialization*** subroutines during program *start-up*: ***GetInput***, ***DataCheck***, and ***Initialize***. ***Initialize*** will call either ***Burn_initial*** or ***Pool_initial*** depending on the ignition source exposing the wall. ***GetInput*** reads the data from an input file called ***Project.Dat***. This file contains all of the needed material properties, the wall dimensions, analysis flags, and time and time step data. There are several analysis flags available. There can be a cone calorimeter simulation, the ignition source can be entirely separated from the heat release rate and flame height calculations, several debug settings exist that dump a number of additional variables to output files, and the ignition source type can be selected. ***GetInput*** is also responsible for reading in the heat of gasification data from the file ***Heat_Gas.Dat***. The subroutine ***DataCheck*** checks the input data to ensure that there are no errors that could potentially cause the program to lock up. If an error is detected, such as a negative temperature or an invalid flame height correlation selection, the program is aborted. Next the driver calls the ***Initialize*** subroutine. This subroutine is responsible for setting the initial values for all the variables. Depending on the ignition source, this subroutine will call either ***Burn_Initial*** or ***Pool_initial*** to further initialize variables specific to the ignition source.

The main calculation loop in the main driver is a triple loop in time and the x and y coordinates. After the first time step the driver calls the subroutines ***GetHG***, ***mlr***, ***SetFlags***, and ***SetFlameHeight***. These subroutines update the status of each element and calculates the current flame height on the wall. Next the driver calls the subroutine flux which determines which surface temperature calculation subroutine to call, ***Secant*** or ***Runge-Kutta***, depending on the overall temperature rise of the element. After all the element surface temperatures have been updated, the driver calls ***EndCheck*** to determine if either the fire has extinguished or all the mass has burned out. If either is true, subroutine ***OutPut*** is called and the program terminates. Otherwise the time is incremented and the procedure repeats. The following is a listing and brief description of the subroutines, functions, and input and output files associated with the flame spread program.

3.1.1 Subroutines and Program Driver

main() - main driver responsible for calling subroutines in order and incrementing time and spatial loops.

GetInput() - Reads Project.Dat and heat_gas.dat input files and stores the data in common blocks.

DataCheck(integer errno) - Checks the input data for errors that may crash the program and if an error is detected, returns the error number.

Initialize() - Initialize variables common to all exposures.

Burn_Initial() - Initialize variables common to only a line burner ignition source.

Pool_Initial() - Initialize variables common to only a pool fire ignition source.

SetFlags(real hr) - Adjusts the flag state for each element. Elements can be in preheat above the flame, in preheat behind the flame, ignited, burned out, or inert (void).

EndCheck(logical mflag) - Determines if either the wall material has been completely consumed or if the fire has burned out and returns a .TRUE. or .FALSE.

Output(real hrr, integer icount) - Writes the necessary output data to flame.dat (flame height and pyrolysis data) and heatreal.dat (heat release rate data). If debug mode is invoked additional files include coords.dat (elemental data) and temps.dat (elemental temperature data) and flux.dat (elemental flux data).

Secant(integer ni, integer nj, integer icount, real qexp, real rtime) - Solves for the surface temperature at time 'rtime' using the constant heat flux equation. This is used only for a specified temperature difference from the initial surface temperature at time 0 to avoid numerical instability.

Runge-Kutta(integer ni, integer nj, real qexp) - Solves the cubic temperature profile differential equation for the surface temperature at time 'rtime'.

flux(integer kflag, integer ni, integer nj, real rtime, integer icount) - Determines the exposure flux for element (ni,nj) and calls the respective surface temperature subroutine.

GetHG(real heat_gas, integer kflag, integer ni, integer nj) - Updates the current heat of gasification value for element (ni,nj) based on the pyrolysis penetration depth.
mlr(real heat_gas, integer kflag, real rmassloss, integer ni, integer nj) - Computes the mass loss rate per unit area for element (ni,nj).

KillBurner() - Shuts off the burner immediately.

TurnBurnerOff(real rtime) - Shuts off the burner after all the material behind the initial burner flame has burned out.

SetFlameHeight(integer nend) - Adjusts the current flame height based on the updated total heat release rate per unit length. If there is no heat release rate (and consequently no flame height), it returns a flag indicating the program should terminate.

GetBurnHeat(real rtime) - Computes the burner heat release rate as a linear interpolation of the final burner heat release rate over some specified time to achieve this maximum.

3.1.2 Functions

real GetFlux(real ycGF) - Calculates the heat flux for an element at a height ycGF using one of several heat flux correlations.

real q_burn(ycQB) - Calculates the burner contribution to the surface incident heat flux if the burner fire was specified as being separate from the wall fire in the input file.

real GetFluxPI(ycGF) - Calculates the burner contribution to the surface incident heat flux if it was specified that the burner use a different heat flux correlation than the wall fire in the input file.

real yc(integer nj) - calculates the absolute y coordinate for element (x,nj).

real xc(integer ni) - calculates the absolute x coordinate for element (ni,y).

3.1.3 Input and Output Files

project.dat - contains input data specifying the analysis type, material properties, dimensions, and desired heat flux and flame height correlations as well as time data.

heat_gas.dat - Contains heat of gasification, depth pairs calculated from Cone Calorimeter data.

tempout - Contains a list of nine elements (specified by vertical number) for which the temperature, time history is desired (used only in debug mode).

heatreal.dat - Contains output heat release, time values.

flame.dat - Contains output flame height, pyrolysis front height, burnout front height, flame height above floor versus time values.

debug.dat - Contains mass loss rate versus time data (output only in debug mode).

flux.dat - Contains elemental net and incident heat flux data versus time (output only in debug mode).

temps.dat - Contains temperature versus time data for nine elements listed in tempout (output only in debug mode).

4.0 RESULTS OF THE MODEL

The model results were compared with full-scale tests to evaluate the capabilities of the computer program in predicting vertical spread. Heat release rates, surface temperatures, and flame heights were compared with data available in the literature. No tests were found that described in adequate detail all of the potential characteristics for comparison. In addition, the test conditions were not adequately described in terms of the ignition temperature, material properties, and heat flux conditions. Comparisons were made using values or data from other literature sources. Comparisons were also made to assess the sensitivity of the model to several parameters, including material properties (thermal inertia (kρc), heat of gasification, ignition and pyrolysis temperature), heat flux and flame height correlations. It was demonstrated that the predictions can be altered significantly using parameters within the bounds of reasonable values. Consequently, a successful prediction relies on accurately assessing these parameters for each case.

Validation of the numerical solution for upward flame spread was made by comparison with full-scale experimental results using material properties from bench-scale data available in the literature. Full-scale data was available for vertical flame spread on polymethylmethacrylate (PMMA), plywood, and wood particle board. The present numerical solution was compared to the experimental measurement of flame spread over a vertical PMMA surface by Wu, Delichatsios, and de Ris (reference (11)), the experimental measurements of flame spread over a vertical surface of plywood with externally applied radiation flux by Delichatsios et al. (reference (12)), and vertical flame spread measurements on wood particle board by Saito, Quintiere, and Williams (reference (13)).

4.1 Model Inputs

The ignition, flame spread properties and dimensions of PMMA, plywood, and wood particle board are tabulated in Table 1. The properties of all materials in Table 1 are based on the bench-scale test data available in the literature. The sources of the data and methods used for this determination are discussed in the subsequent sections.

Table 1. Properties and Dimensions of Selected Material

Material*	Height H m	Width W m	Thickness Δ m	Ignition temp T_{ig} °C	Pyrolysis temp T_p °C	Thermal inertia kρc $(kW/m^2 K)^2$ sec	Density ρ kg/m^3	Heat of combustion Δh_c kJ/kg	Heat of gasification Δh_g kJ/kg
PMMA	0.90 (11)	0.20 (11)	0.0245 (11)	320 (10)	377	0.60 Deduced	1200 (17)	25000 (19)	1600 (16)
PMMA	5.0 (11)	0.58 (11)	0.0245 (11)	320 (10)	377	0.60 Deduced	1200 (17)	25000 (19)	1600 (16)
Plywood	2.40 (12)	0.61 (12)	0.0127 (12)	350 (22)	427	0.475 Deduced	473 (22)	15000 (22)	6850 Deduced
Wood Particle Board	1.80 (13)	0.30 (13)	0.013 (13)	350 (13)	427	0.475 Deduced	600 (10)	14000 (10)	6850 Deduced

* - Numbers in parenthesis indicate reference number as listed in Section 8.0.

Data relevant to the prediction of flame spread on a material has been derived experimentally by several investigators. Experimental results by Kashiwagi and Ohlemiller (reference (14)) for the radiant heating of PMMA (Rohm and Hass Type G) in a nitrogen atmosphere leads to a leveling of the surface temperature as vaporization occurs. For PMMA, these temperatures ranged from 300-330°C for a heat flux of 17 kW/m^2 and 365-380°C for 40 kW/m^2.

Tewarson and Pion (reference (15)) and Jackson (reference (16)) conducted mass loss experiments for estimating the steady or time-averaged burning rate in terms of heat of gasification, Δh_g, for PMMA (Rohm and Hass Type G). The heat of gasification corresponding to the Jackson (reference (16)), 1600 kJ/kg, is used in this model.

The density of PMMA has been measured by Quintiere and Harkleroad (reference (10)), and Agrawal and Atreya (reference (17)) as well as by Tewarson and Ogden (reference (18)) and ranged from 1190-1200 kg/m^3. Tewarson (reference (19)) has measured flammability parameters of materials associated with combustion and flame spread. In the experiments, the heat of combustion, Δh_c, was measured to be 24,900 kJ/kg for PMMA. These properties were used to make the predictions for upward flame spread for PMMA.

The thermal inertia ($k\rho c$) of PMMA was found by fitting ignition data of Quintiere and Harkleroad (reference (10)) using an ignition temperature of 320°C (reference (13)). The calculated value of $k\rho c$ from Quintiere and Harkleroad (reference (10)) ignition data was 0.60 $(kW/m^2\text{-}K)^2$ sec, which is in agreement with the value of 0.57 $(kW/m^2\text{-}K)^2$ sec reported by Tewarson and Ogden (reference (18)), 0.61 $(kW/m^2\text{-}K)^2$ sec obtained by Delichatsios, Panagiotou, and Kiley (reference (20)), and 0.61 $(kW/m^2\text{-}K)^2$ sec reported by Orloff, de Ris, and Markstein (reference (21)). There were few data available on the material's pyrolysis temperature. A value 50°C - 60°C greater than the ignition temperature is representative of the available data.

The ignition and flame spread properties for plywood and wood particle board were deduced from the experimental bench-scale data of Quintiere and Harkleroad (reference (10)), Janssens (reference (22)), Parker (reference (23)) and Quintiere (reference (7)). The thermal inertia was calculated by fitting critical ignition heat flux data as was done with the PMMA. Fig. 9 and Table 2 compare the predicted and actual ignition times (from Quintiere and Harkleroad, 1985 (reference (10)) using an ignition temperature of 350°C as reported by Janssens, 1991 (reference (22)) and a thermal inertia of 0.475 $(kW/m^2\text{-}K)^2$ sec.

Table 2. Comparison of Experimental and Predicted Ignition Time for Plywood (reference (10))

$k\rho c = 0.475$ $(kW/m^2\text{-}K)^2$ sec (Deduced Value)	$T_{ig} = 350$ (°C), $T_p = 427$ (°C), Janssens, 1991 (Reference (22))	
Experimental heat flux exposure (kW/m^2)	Measured ignition time (sec)	Predicted ignition time (sec)
17	308	310
20	185	189
24	115	114
30	62	65
41	30	31
51	21	20

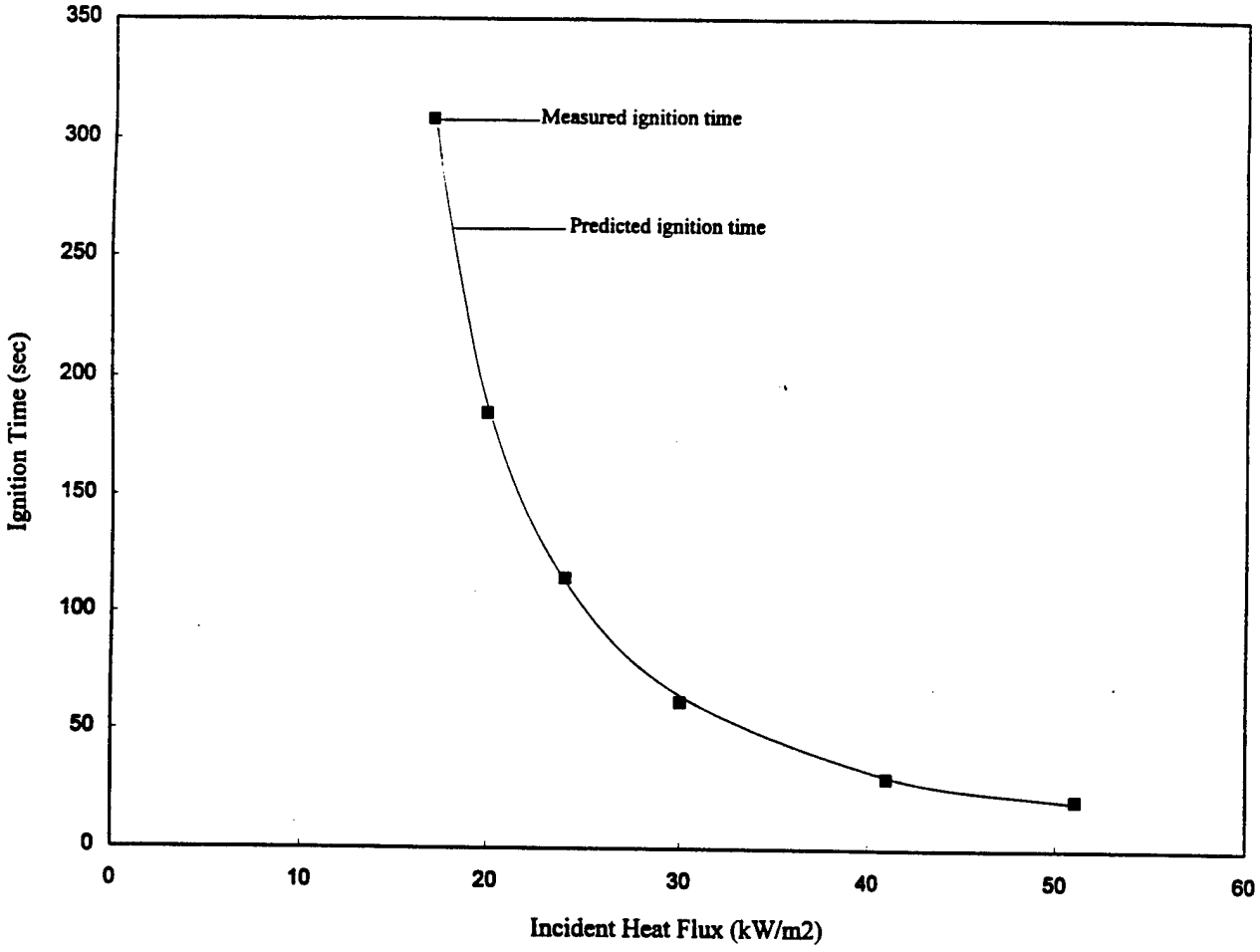

Figure 9 Incident heat flux versus measured and predicted ignition time for plywood at $k\rho c = 0.475$ (kW/m^2 K)^2 sec and $T_{ig} = 350$ °C.

The heat of gasification for plywood was deduced from the experimental results of Janssens (reference (22)) and Parker (reference (23)). This was done by holding all material properties (Table 1 and Appendix A3 for plywood) constant and varying the heat of gasification until all of the data were matched satisfactorily. The pyrolysis temperature for wood was given in Janssens (reference (22)) as 427°C. Table 3 compares the measured and predicted heat release rate with Δh_g = 6850 kJ/kg at several external flux levels.

Table 3. Comparison of experimental and predicted heat release rate results for plywood at Δh_g = 6850 kJ/kg (deduced value)

Experimental heat flux exposure (kW/m^2)	Average heat release rate (kW/m^2)	Predicted heat release rate (kW/m^2) Δh_g = 6850 kJ/kg (Deduced Value)
25 [22]	85.20	84
35 [22]	104.10	104
50 [22]	142.10	135
50 [23]	124.0	135
60 [22]	156.30	155

Wood particleboard was assumed to have the same material properties as plywood with the exception of the thermal inertia. As with the PMMA and the plywood, this value was estimated by fitting the data of Quintiere (reference (7)). It was determined that the same thermal inertia ($k\rho c$ = 0.475 $(kW/m^2\text{-}K)^2$ sec) estimated for plywood is also appropriate for particleboard. A comparison of the measured and predicted ignition times for wood particleboard with $k\rho c$ = 0.475 $[kW/m^2\text{-}K]^2$ sec and Tig = 350°C is given in Table 4.

Table 4. Comparison of Experimental and Predicted Ignition Time for Wood Particleboard (reference (7))

$k\rho c = 0.475$ (kW/m^2-K)^2 sec (Deduced Value)	$T_{ig} = 350°C$, $T_p = 427°C$ (reference (13))	
Heat Flux (kW/m^2)	Measured ignition time (sec)	Predicted ignition time (sec)
20	245-258	399
25	155-180	199
30	80-110	120
36	68	75
40	60	58
45	49	45
50	40	35
58	30	26
60	31	24
65	18	20

4.2 Comparison of Predicted with Experimental Results for Non-charring Polymethylmethacrylate (PMMA)

Wu, Delichatsios, and de Ris (reference (11)) conducted experiments to measure heat release rate for bench-scale and full-scale PMMA wall fires. In the bench-scale tests, a vertical PMMA slab measuring 0.90 m high, 0.2 m wide and 25 mm thick was ignited at the bottom of the panel by 20 ml of methanol and cotton balls in an aluminum dish (0.025 m x 0.20 m x 0.01 m high). The full-scale flame spread experiments were carried out with a 25 mm thick PMMA slab, 0.58 m wide x 5 m high. The ignition source was 35 ml of heptane in a copper dish (0.025 m x 0.6 m x 0.025 m high) at the bottom of the wall. This was simulated in the model as a 1 kW/m line fire source.

Fig. 10 shows a comparison of heat release rate during upward flame spread over 0.90 m x 0.20 m vertical PMMA surface (refer to Appendix A, Table A-1 for the input data). The solid line is the model prediction while the dashed line is the experimental data of Wu, Delichatsios, and de Ris (reference (11)). The properties listed in Table 1 were used for the PMMA. Due to the sensitivity of the computer model to the heat flux and flame height correlations, several simulations of the test were perform in order to determine the optimum combination. The results in Fig. 6 show reasonable agreement with experimental data using the flame height correlation given by $y_f = 0.052\ Q'^{2/3}$ [Delichatsios (reference (4))], and the flame heat flux correlation given by Equations (7) & (8) in Section 2.2. The flame heat flux in the burning region was 21 kW/m^2. Exact values of flame heat flux after ignition were not described in the test conducted by Wu, Delichatsios, and de Ris (reference (11)). A value of 21 kW/m^2 heat flux after ignition was found to yield the best fit. It should be noted that the heat flux from the flame to the wall in the burning region is not actually constant but rises to some peak value then declines.

Fig. 11 compares the predicted heat release rate and the measured heat release rate for a 5.0 m x 0.58 m vertical surface of PMMA (Wu, Delichatsios, and de Ris (reference (11)). The input file is listed in Appendix A. The solid line represents the model prediction and the dashed line shows the experimental results. The flame height correlation used to model the full scale test was $y_f = 0.0666\ Q'^{2/3}$, developed by Tu, and Quintiere (reference (5)). The flame height correlation gives a slightly larger flame height than the one used to model the bench-scale tests and indicates that the size of the test may influence the height of the flame for a given heat release rate per unit area. The heat flux correlation used in the full-scale test predictions is given by Equations (7) and (8). A 31 kW/m^2 heat flux was used after the material ignited. As with the flame height correlation, the heat flux was greater than in the bench-scale tests.

4.3 Comparison of Predicted and Experimental Results for Plywood

Delichatsios et al. (reference (12)) have conducted a theoretical and experimental analysis of upward fire spread along 2.4 m high, 0.61 m wide and 12.7 mm thick vertical plywood wall. Five full-scale flame spread experiments were conducted. The samples were exposed to a specified heat flux from a large-scale radiant panel. The following measurements were made:

(1) Rate of heat release,
(2) Total heat flux to the specimen surface,
(3) Surface temperature, and
(4) Propagation of the pyrolysis front.

The full-scale test results demonstrated the sensitivity of the flame spread rate to the external heat flux. The samples of plywood in the experiments were ignited by a red-hot nichrome wire. The wire was preheated using a welder power supply set to provide a 40 Amp current through the wire. After preheating, the wire was brought into direct contact with the specimen at a location approximately 25 mm above the base of the specimen. A thin spacer located between specimen holder and the center of the specimen was used to make the specimen slightly convex at the base and ensure good contact for the ignition wire over the entire width of the specimen.

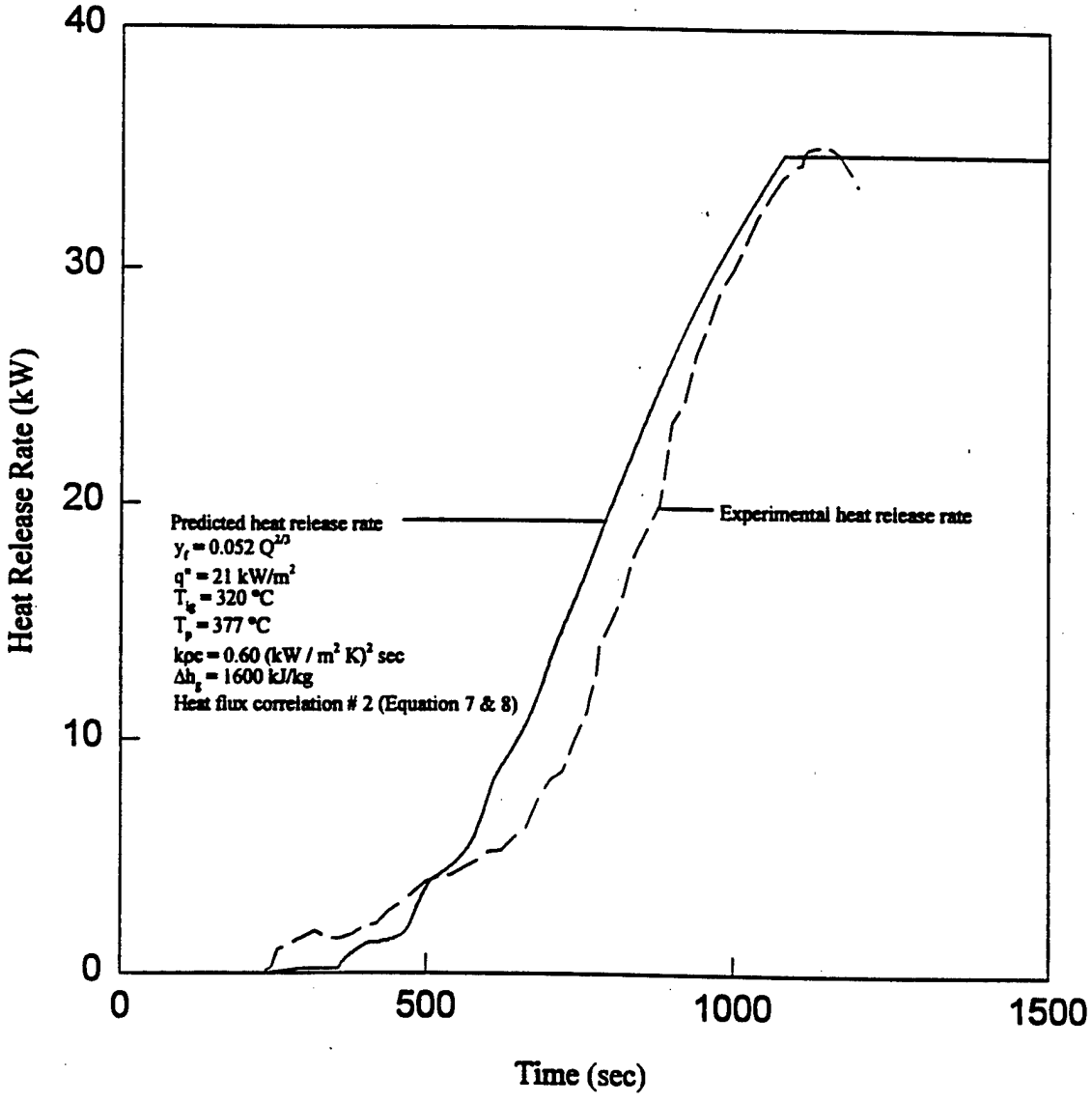

Figure 10 Comparison of heat release rate predictions for a 0.90 m x 0.20 m vertical PMMA surface with Wu, Delichatsios, and de Ris, 1993 data (reference (11))

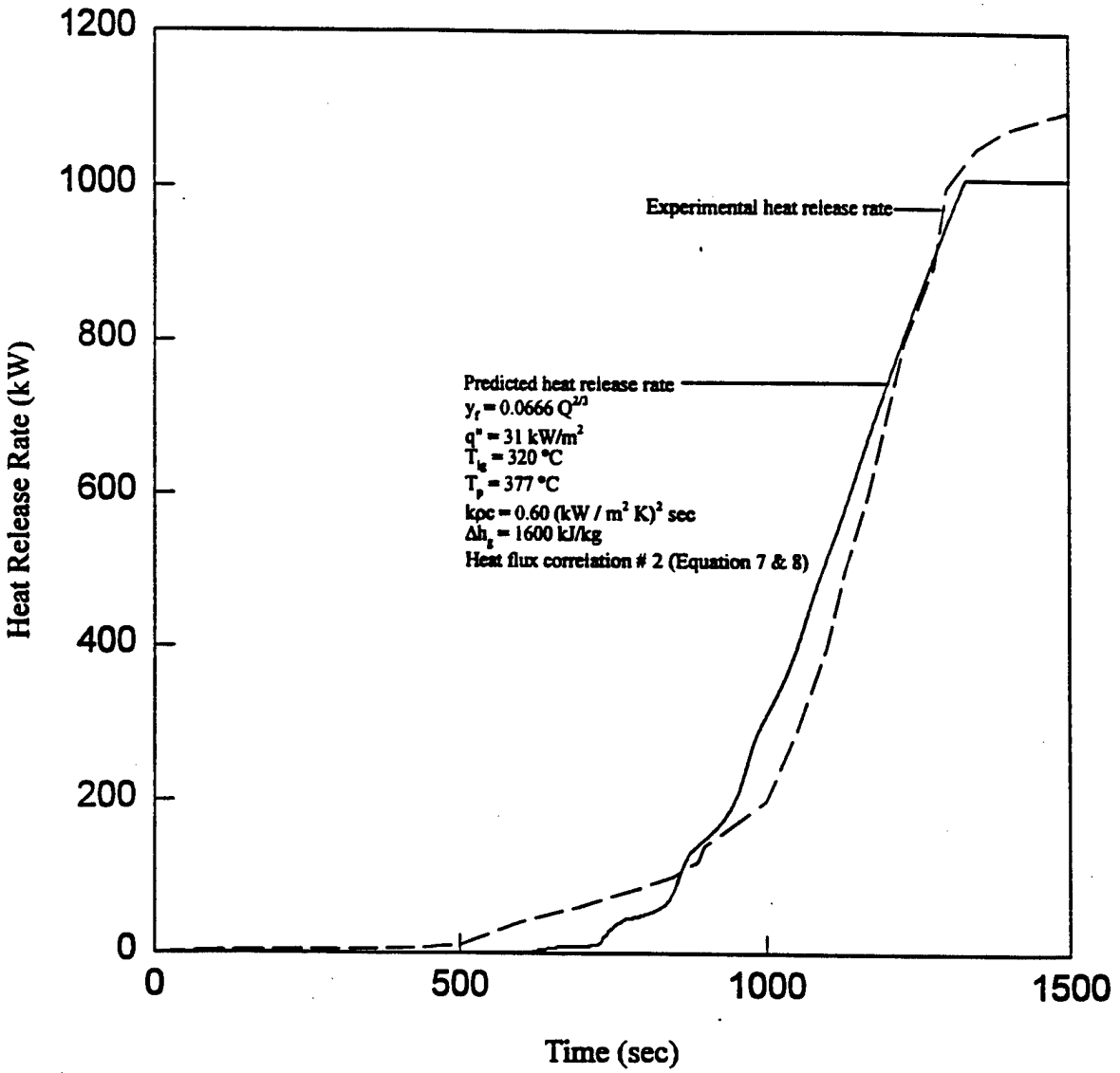

Figure 11 Comparison of heat release rate predictions for a 5.0 m x 0.58 m vertical PMMA surface with Wu, Delichatsios, and de Ris, 1993 data (reference (11))

Comparisons of the upward flame spread model to the full-scale experimental results (Delichatsios et al. (reference (12)) are shown in Fig. 12 and 14. The properties of plywood used for the prediction were discussed in Section 4.1. The heat release rate during pyrolysis was predicted and compared to the measured results in Fig. 12, (refer Appendix A, Table A-3, test 1 for input data) for good-one-side (GIS) plywood. In Fig. 12, the agreement with the experimental measurement is very good. Typical measured peak heat release rate results in this test series, along with the predicted peak heat release rate results, are summarized in Table 5. Fig. 13 shows the heat release rate curves obtained from the computer model for each type of plywood.

Table 5. Comparison of Experimental and Peak Heat Release Rate Results (reference (12))

Test #	Plywood Type	Heat Flux Exposure (kW/m^2)	Peak Heat Flux (kW/m^2)	Initial Surface Temperature (°C)	Measured Peak Heat Release Rate (kW)	Predicted Peak Heat Release Rate (kW)
1	GIS	5.2	34-40	160	118	114
2	RG	11	45-50	250	250	136
3	RG	7.5	40-45	205	130	124
4	GIS	4.8	33-38	155	105	100
5	GIS	7	40-45	200	175	123

GIS - Good-one-side
RG - Rough grade

The predicted and experimental propagation of the pyrolysis front (determined using surface thermocouples) are shown in Fig. 14. In general, there is a reasonable agreement between predicted and measured propagation of the pyrolysis zone.

Fig. 15 shows the temperature rise history of the specimen with a uniform external flux of 5.2 kW/m^2 over a period of 1200 sec (20 min). The temperature rise and steady preheat temperature were well predicted by the model.

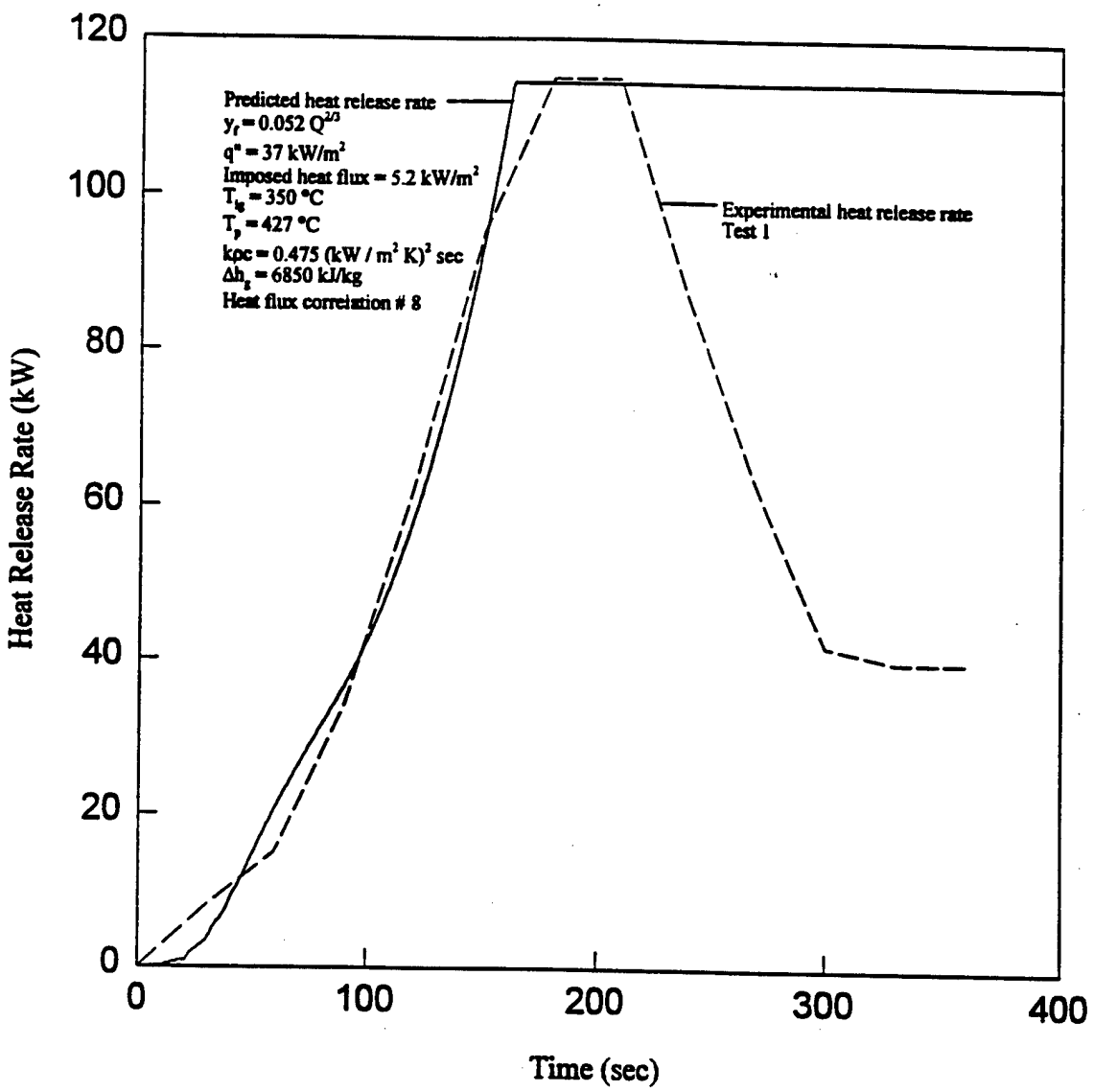

Figure 12 Comparison of heat release rate predictions for a 2.4 m x 0.61 m vertical plywood surface with Delichatsios et al. 1994 data (reference (12))

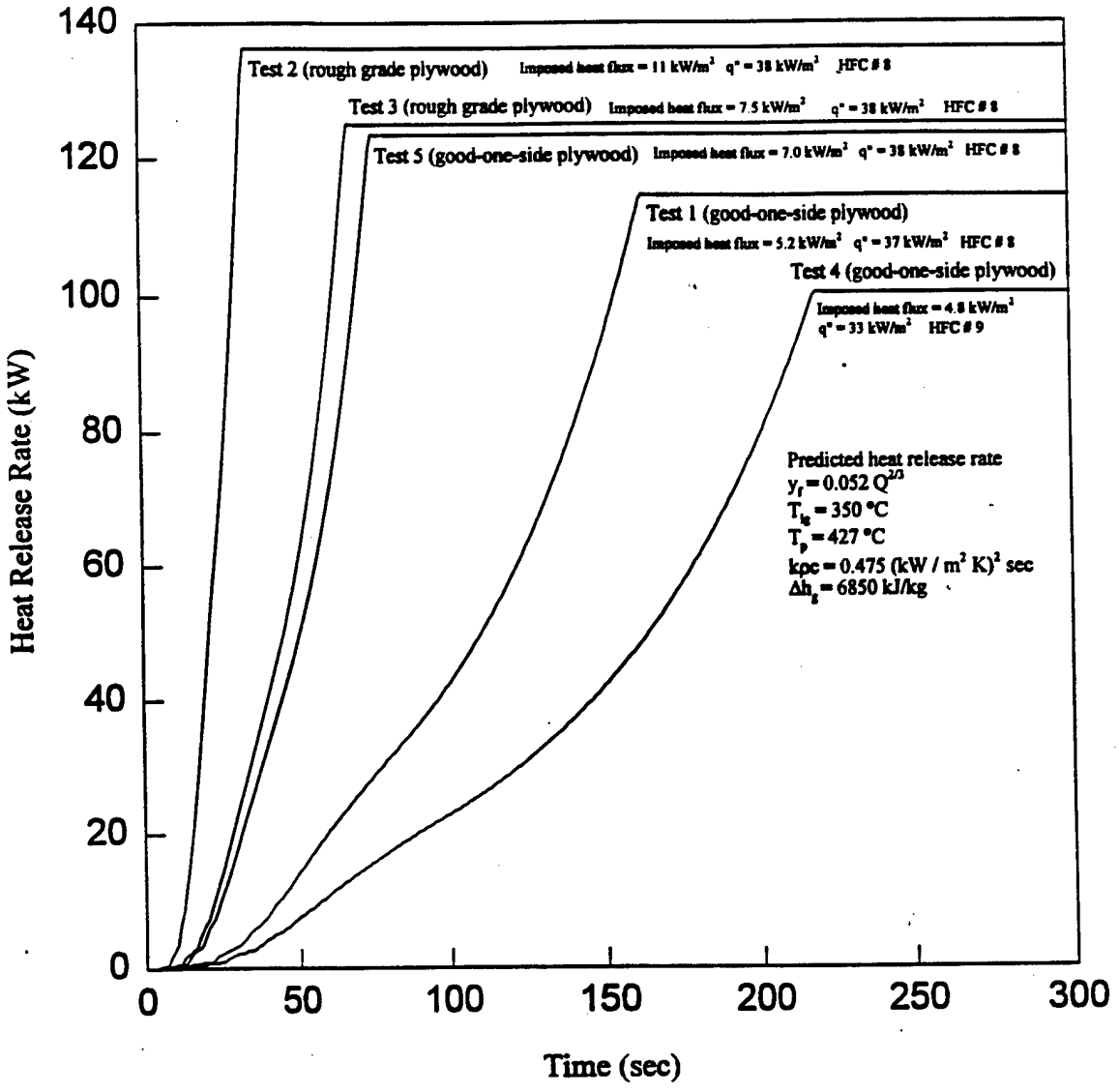

Figure 13 Predicted heat release rate for a 2.4 m x 0.61 m vertical plywood surface (reference (12))

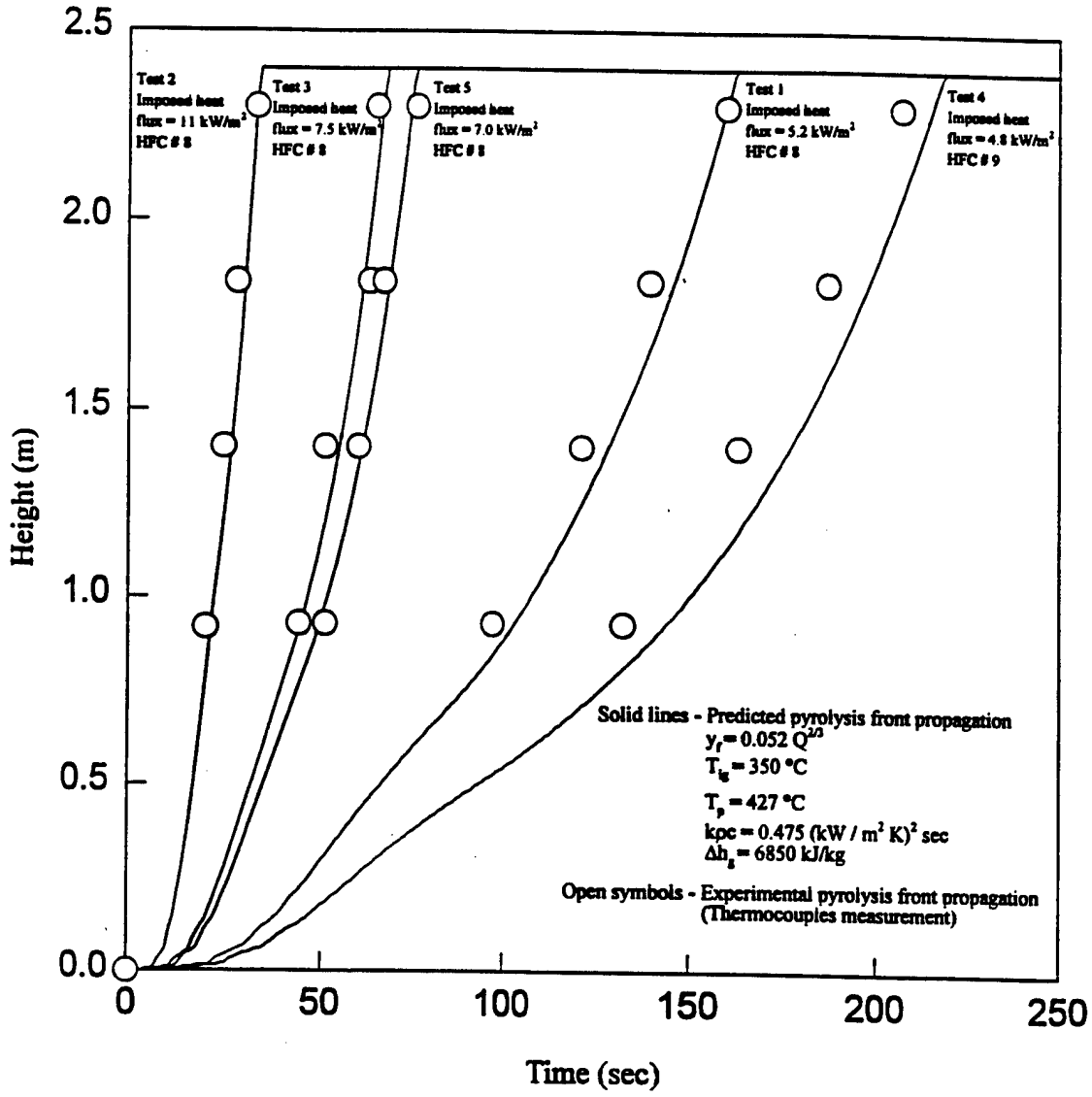

Figure 14 Comparsion of pyrolysis front propagation predictions for a 2.4 m x 0.61 m vertical plywood surface with Delichatsios et al. 1994 data (reference (12))

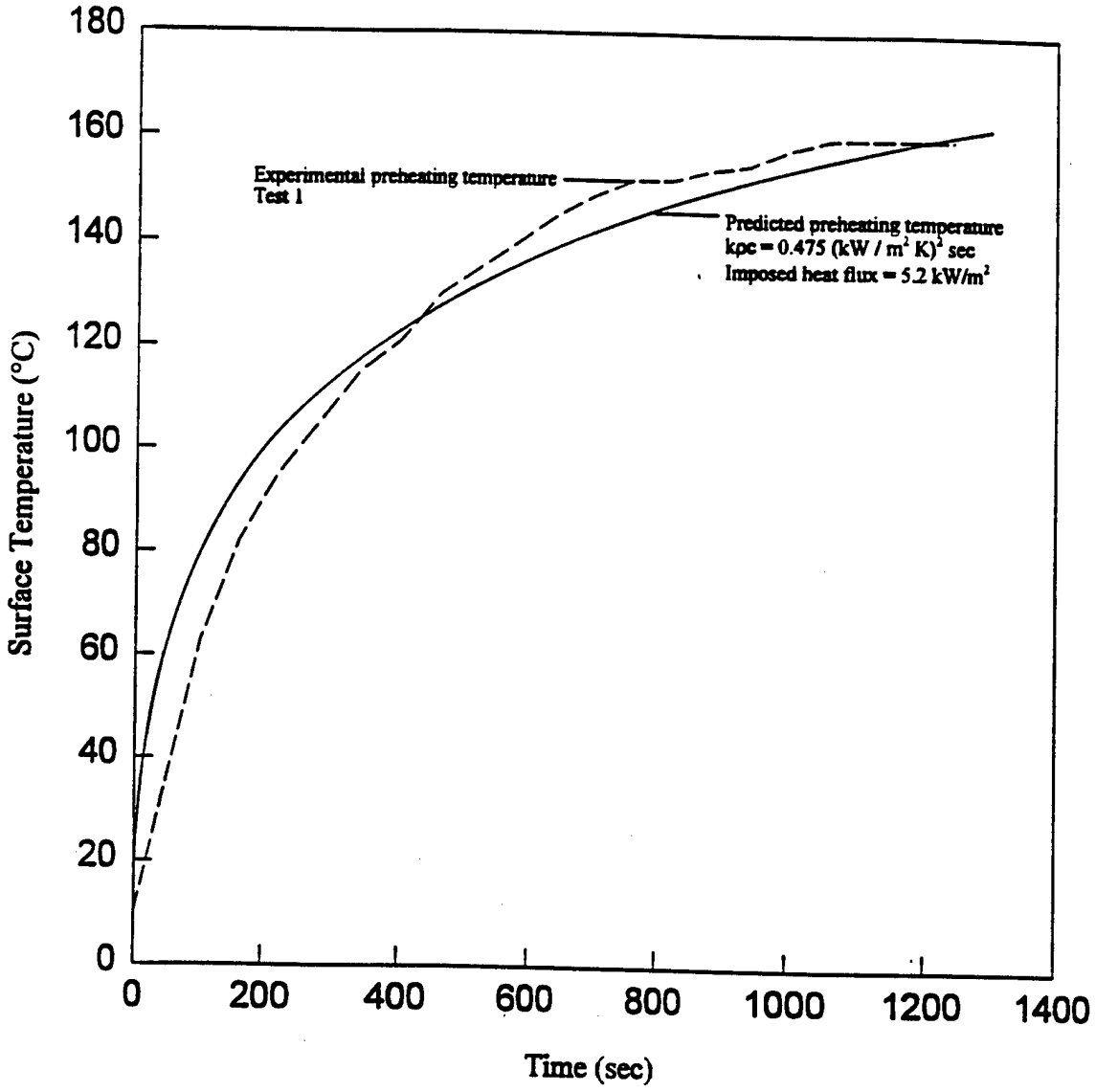

Fig. 15 Comparison of preheating temperature prediction for a 2.4 m x 0.61 m vertical plywood surface with Delichatsios et al. 1994 data (reference (12))

The total flame heat flux after ignition was measured by Delichatsios et al.(reference (12)) for each experiment. For the prediction of heat release rate for each specific test in Figs. 12 - 14, the heat flux after ignition is calculated as average peak heat flux minus imposed heat flux from Table 5. Peak heat fluxes after ignition for all tests conducted by Delichatsios et al. (reference (12)) were greater than heat flux data summarized by Quintiere (reference (7)) (refer Section 2.2 Fig. 3). Based on Fig. 3, five more heat flux correlations have been developed and are shown in Fig. 16, with correlations 1, 2, and 3 discussed in Section 2.2. Correlation 6, 7, 8, 9, and 10 in Fig. 16 all lie above the heat flux plateau in Fig. 3. Table 6 shows heat flux after ignition calculated from Table 5 with heat flux correlation used by the model to compare heat release rate for each test conducted by Delichatsios et al. (reference (12)). The flame height correlation given by Equation (2) in Section 2.2 with $C_f = 0.052\ m^{5/3}/kW^{2/3}$ was used.

Table 6. Heat Flux after Ignition and Heat Flux Correlation for Plywood

Test #	Imposed Heat Flux (kW/m^2)	Heat Flux after Ignition (kW/m^2)	Heat Flux Correlation
1	5.2	37	8
2	11	38	8
3	7.5	38	8
4	4.8	33	9
5	7.0	38	8

4.4 Comparison of Predicted and Experimental Results for Particle Board

Saito, Quintiere, and Williams (reference (13)) have examined the mechanisms and rate of upward flame spread along thermally thick vertical sheets for both charring and non-charring fuels. Measurements of spread rates, flame heights and of surface temperature histories were reported for PMMA and Douglas-fir particle board for flames initiated and supported by a line source gas burner located at the base of the panels. The heat release rate of the burner was varied from 8 kW/m to about 100 kW/m. The pyrolysis front was determined from surface temperature measurements along the sample vertical centerline and flame heights were determined visually. The sustained flame spread was not observed for wood particle board samples even if the burner was left on for ten minutes in the experiments conducted by Saito, Quintiere, and Williams (reference (13)). The maximum height of the char yield (pyrolysis front) increased appreciably with increasing burner energy supply.

The properties of wood particle board (1.8 m high, 0.30 m wide and 13 mm thick) discussed in Section 4.1 (refer to Table 1 and Appendix A) were used to make the predictions shown in Fig. 17 and Table 7 for various intensities of the line burner.

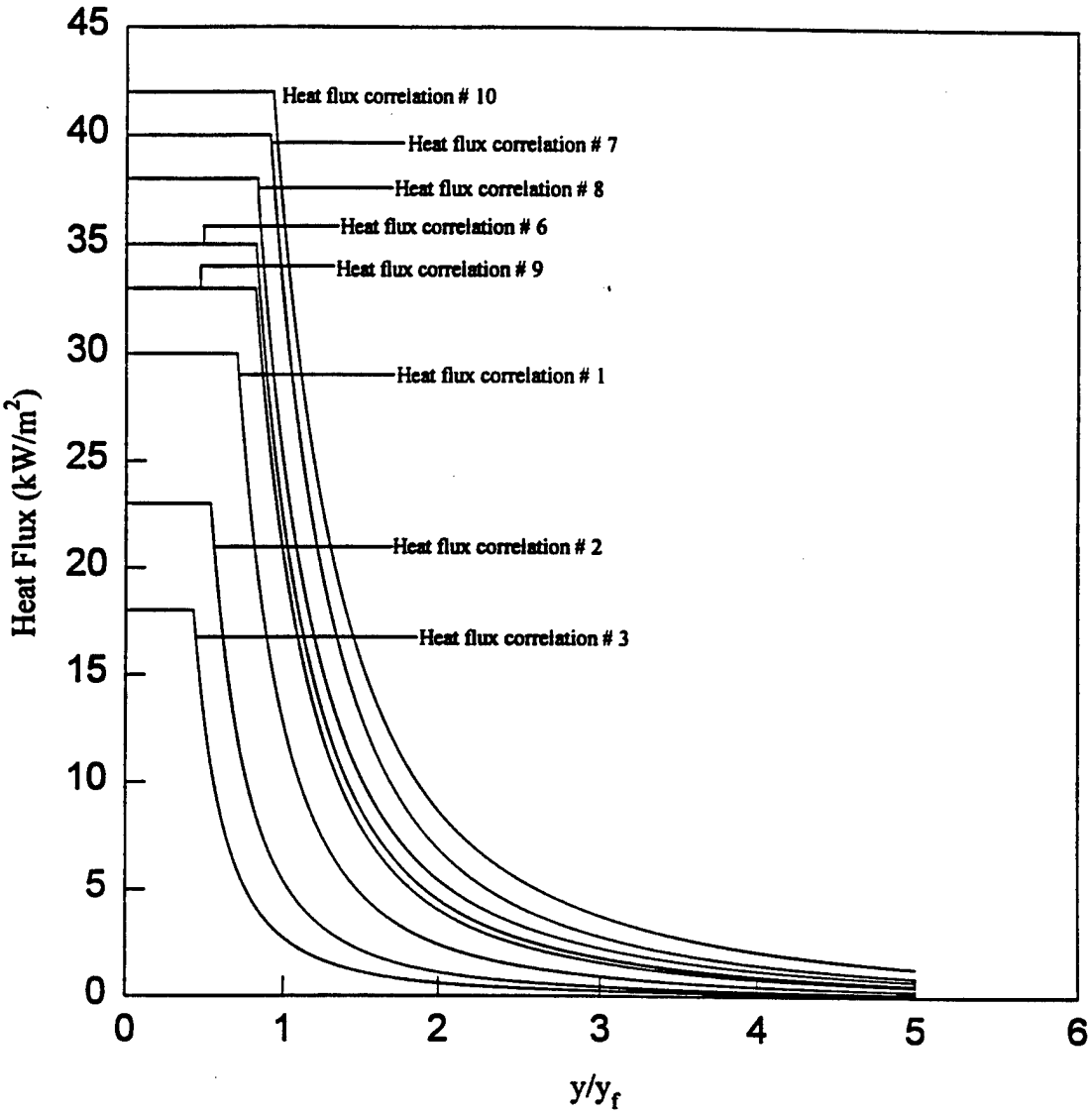

Figure 16 Heat flux correlation for the model

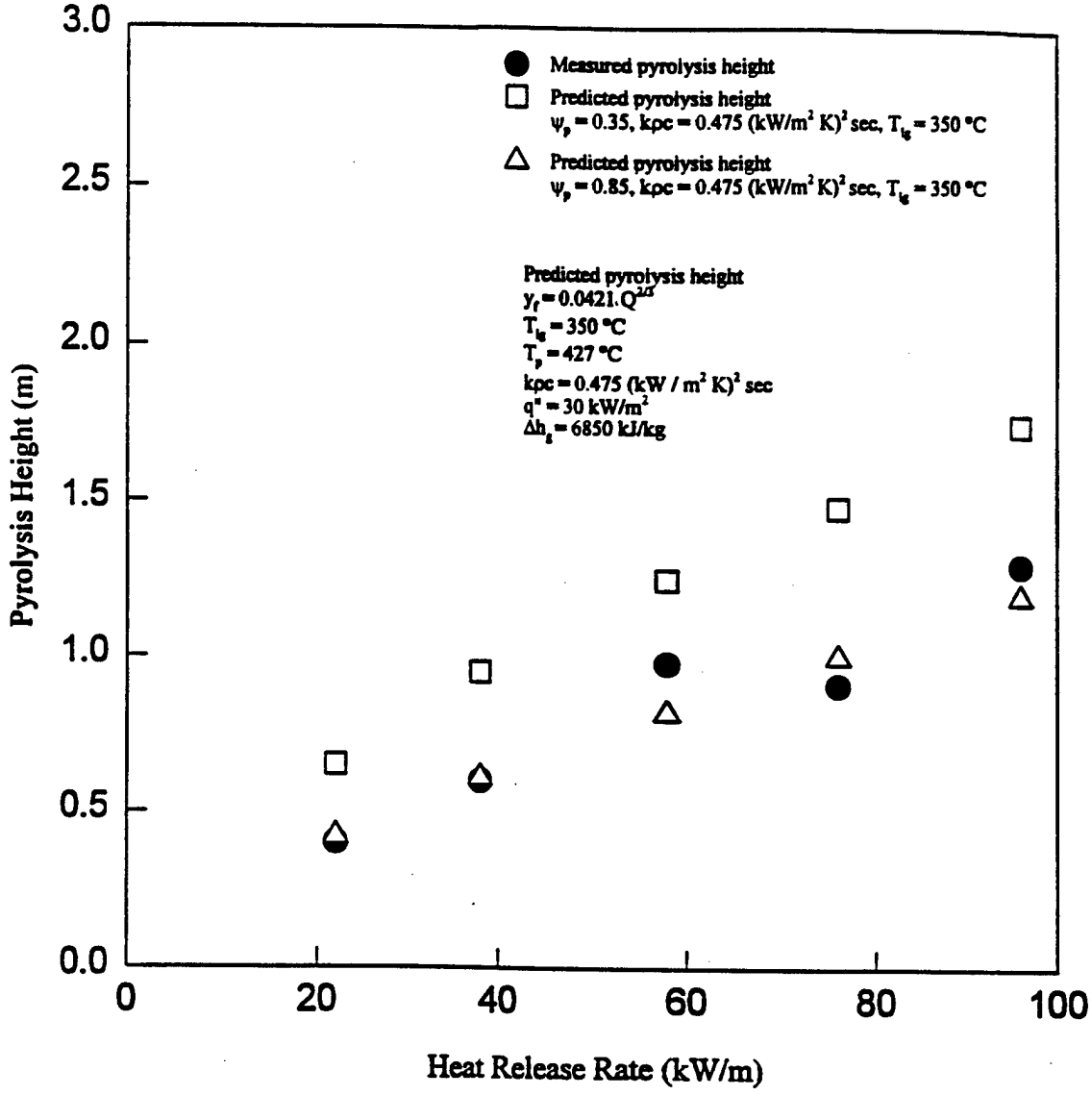

Figure 17 Comparison of pyrolysis height predictions for a 1.8 m x 0.3 m vertical wood particle board with Saito, Quintiere, and Williams, 1985 data (reference (13))

Ignition by the line burner at the base of the particle board sample at various energy releases was simulated by a uniform constant distribution of heat flux to the surface over the flame height. The flame height correlation used to compare the prediction with data is directly obtained from the data reported by Saito, Quintiere, and Williams (reference (13)). Their results show a value of $C_f = 0.0421\ m^{5/3}/kW^{2/3}$ agree with a 2/3 power dependence of the flame height on the heat release rate per unit length. The flame height is as follows:

$$y_f = 0.0421\ \dot{Q}'^{\frac{2}{3}} \tag{24}$$

The predicted maximum pyrolysis heights using a char yield (Ψ) of 0.35 (reference (24)) do not agree with the experimental data quantitatively. They do, however, have a similar trend (slope in the data). Setting the char yield to 0.85 produces results in better agreement with the experimental data of Saito, Quintiere, and Williams (reference (13)). This indicates that, although there is some consistent reproducible aspect to the experimental data, one or more phenomena are not actually being predicted and are being compensated through an unrealistically high char yield.

Table 7. Comparison of Experimental and Predicted Pyrolysis Height Results for Wood Particle Board (reference 13))

Rate of heat release (line fire gas burner) (kW/m)	Measured maximum pyrolysis height (Ψ) (m)	Predicted maximum pyrolysis height (Ψ) (m) $\Psi = 0.35$, $T_{ig} = 350°C$ $k\rho c = 0.475$ $(kW/m^2\ K)^2 sec$	Predicted maximum pyrolysis height (Ψ) (m) $\Psi = 0.85$, $T_{ig} = 350°C$ $k\rho c = 0.475$ $(kW/m^2\text{-}K)^2 sec$
22	0.40	0.65	0.42
38	0.60 - 0.61	0.95	0.61
58	0.91 - 0.98	1.25	0.82
76	0.91	1.48	1.0
96	1.3	1.75	1.2

4.5 Sensitivity Analysis

The rate of flame spread over a material surface is influenced by a number of parameters as discussed in preceding sections. Some of these parameters have a greater impact than others, and consequently more attention should be given to these when modeling a particular situation. This section systematically explores the impact on the model results for seven of the input parameters:

(1) Heat of gasification,
(2) Thermal inertia,

(3) Ignition temperature,
(4) Pyrolysis temperature,
(5) Flame height correlation,
(6) Flame heat flux correlation, and
(7) Flame heat flux after ignition.

The baseline case selected was the small-scale PMMA predicted results (Fig. 10). All parameters were held constant except for the one that was being examined. The sensitivity to the seven parameters is depicted in Figs. 18 - 24.

The effects of variations in the heat of gasification are shown in Fig. 18 in which predictions for heat of gasification from the actual value of 1600 kJ/kg to 2000 kJ/kg are shown. As the Figure illustrates, variations of this relatively small magnitude have a significant effect on the results. This points to the need for excellent characterization of the material properties to allow accurate predictions.

The effects of variations in the thermal inertia from the actual value of 0.6 $(kW/m^2K)^2$ to 0.84 $(kW/m^2K)^2$ are shown in Fig. 19. The sensitivity of the results to variations in the thermal inertia is shown to be less than that associated with the heat of gasification. As the discussion of the inputs in Section 4.1 indicated, the heating and ignition behavior of materials can typically be well represented by the integral heat transfer model and the ignition temperature concept. As such, significant uncertainties in the ignition response as represented by the thermal inertia and ignition temperature are not expected. Figure 20 shows the effect of varying the ignition temperature input. It is possible to determine the ignition temperature to within 20°C so that significant errors due to ignition temperature uncertainties are not large. It needs to be remembered that the thermal inertia and ignition temperature are used together to predict the ignition of each numerical element. Thus, the real key to assessing the uncertainties is the degree of fit in the time to ignition over a range of heat fluxes as shown in Fig. 9.

The effects of pyrolysis temperature on the heat release rate are shown in Fig. 21. The pyrolysis temperature primarily governs the radiative heat losses from the burning surface. For some materials like PMMA, the surface temperature during burning is quite constant. Other materials like wood can experience variations in surface temperature during burning in excess of 100°C. As such, the uncertainties associated with the use of a constant pyrolysis temperature can vary widely depending on the material. This variable may be responsible for the difficulties in predicting the flame spread distances on the wood particleboard tests.

The effect of the flame height correlation constant is demonstrated in Fig. 22. The range of constants examined in Fig. 22 corresponds to the range of constants reported in the literature. As the Figure shows, this constant can markedly affect the results of the prediction. Additional detailed investigation of wall flame height correlations is indicated by this sensitivity.

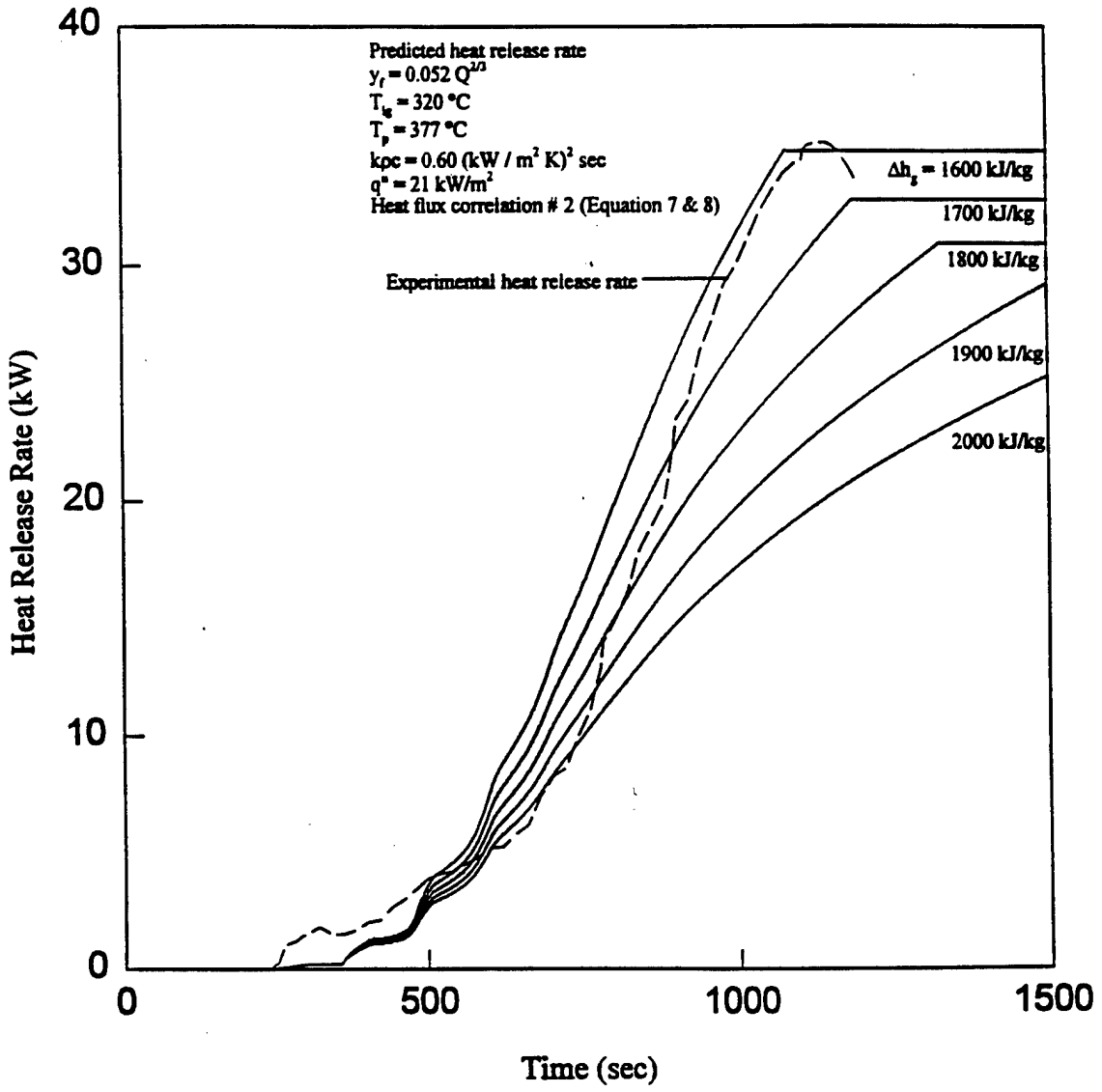

Figure 18 Comparison of heat release rate predictions for a 0.90 x 0.20 m vertical PMMA surface at different values of heat of gasification with Wu, Delichatsios, and de Ris, 1993 data (reference (11))

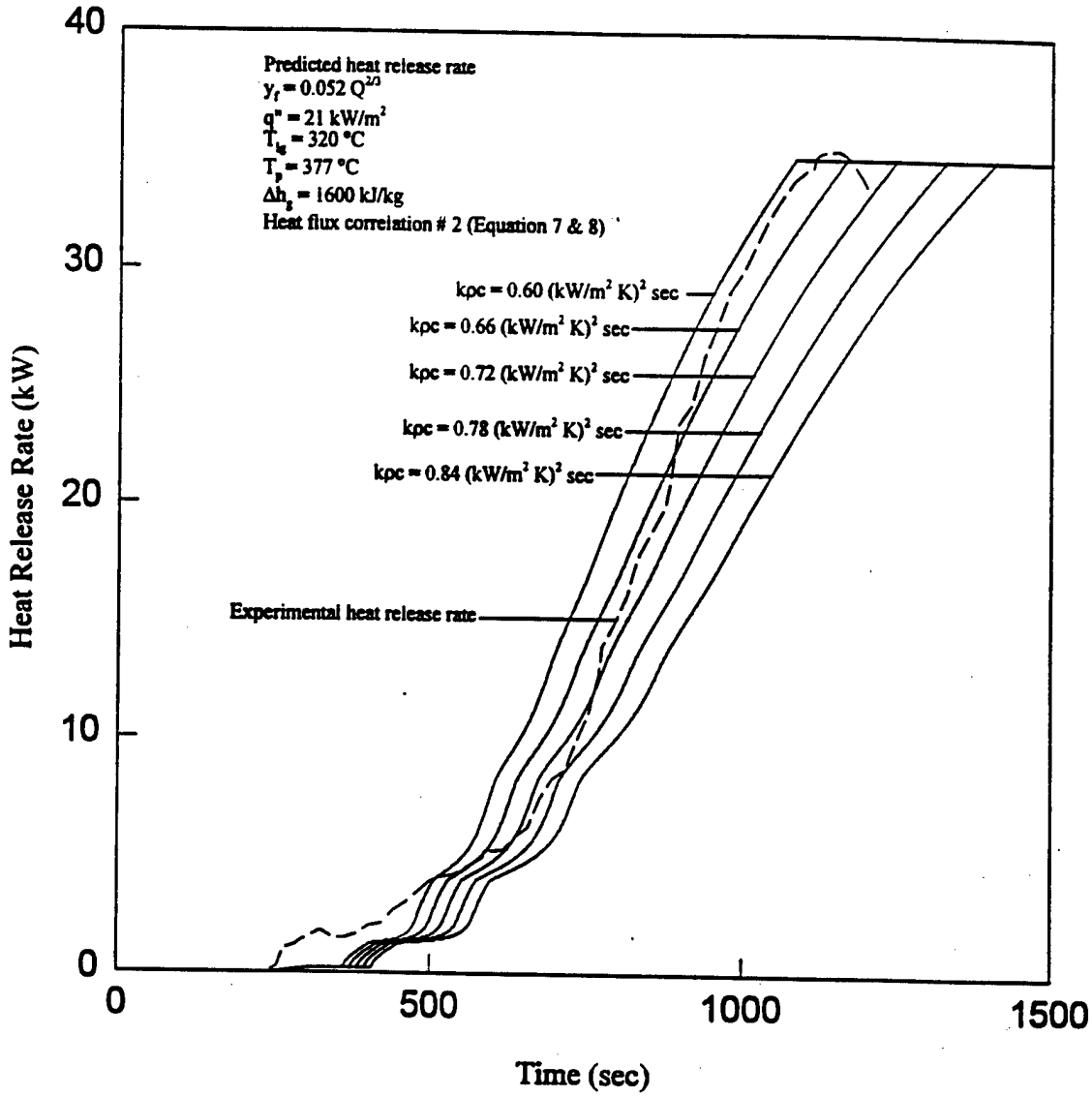

Figure 19 Comparison of heat release rate predictions for a 0.90 m x 0.2 m vertical PMMA surface at different values of thermal inertia with Wu, Delichatsios, and de Ris, 1993 data (reference (11))

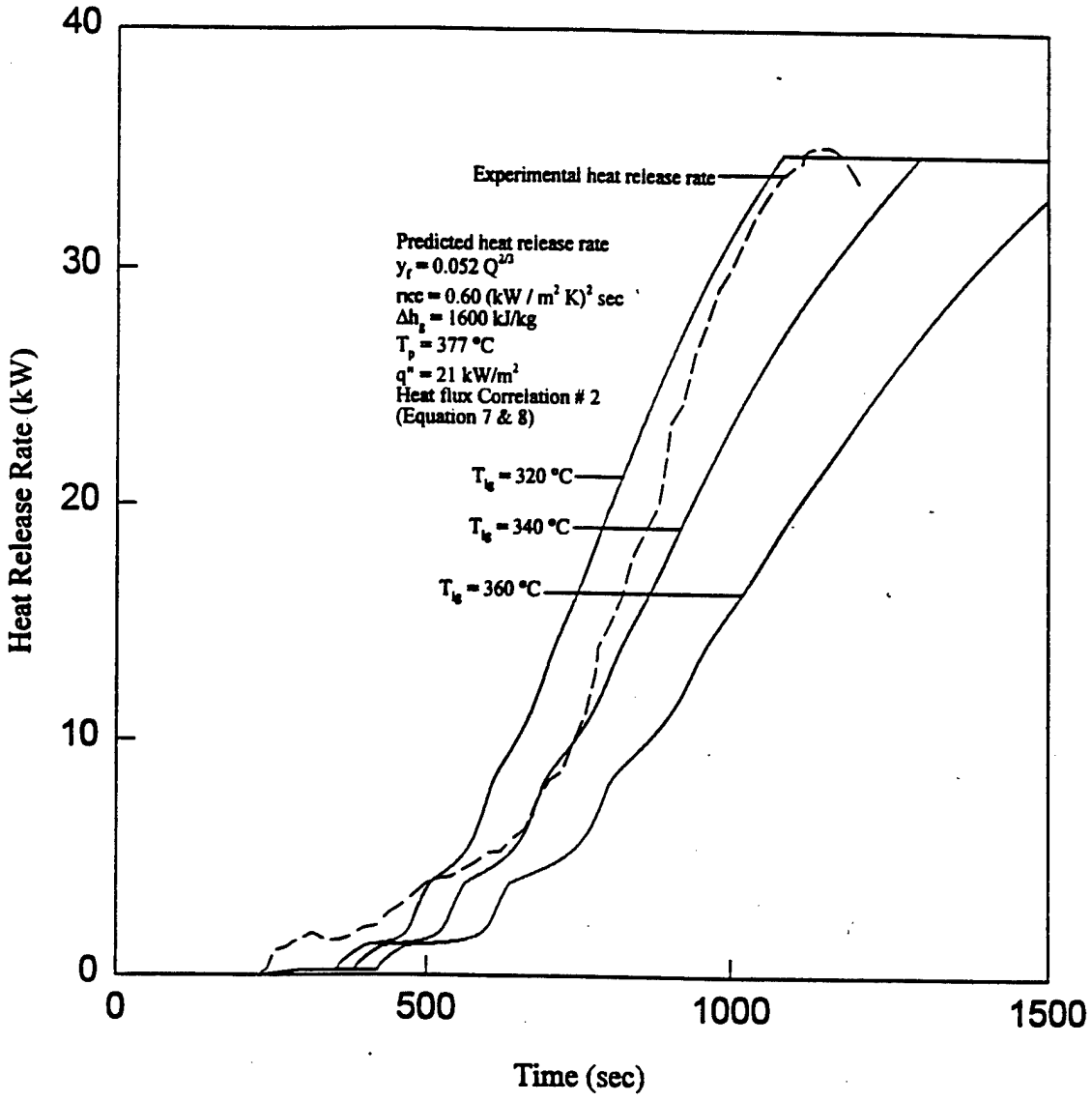

Figure 20 Comparison of heat release rate predictions for a 0.90 m x 0.20 m vertical PMMA surface at different ignition temperature with Wu, Delichatsios, and de Ris, 1993 data (reference (11))

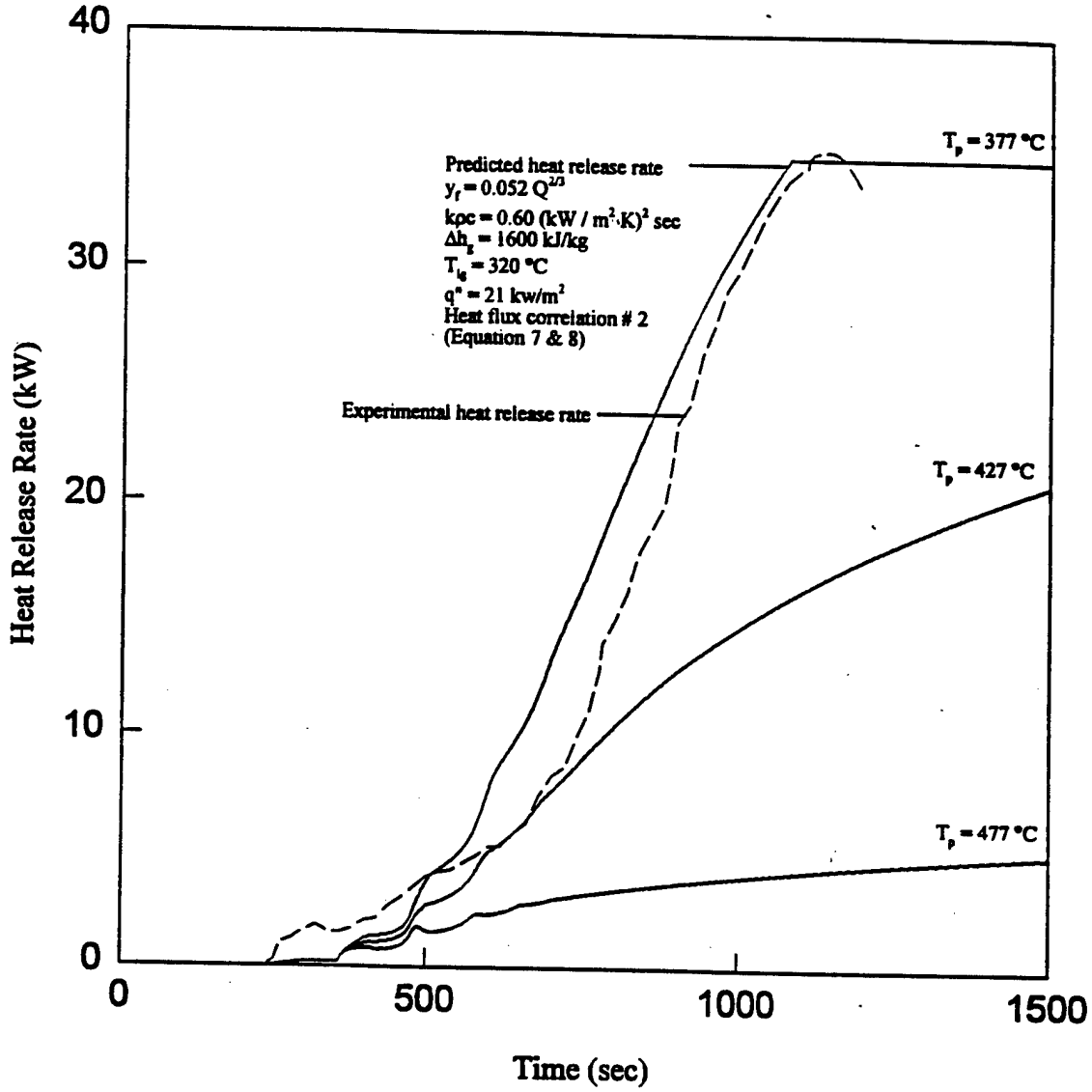

Figure 21 Comparison of heat release rate predictions for a 0.90 m x 0.20 m vertical PMMA surface at different pyrolysis temperature with Wu, Delichatsios, and de Ris, 1993 data (reference (11))

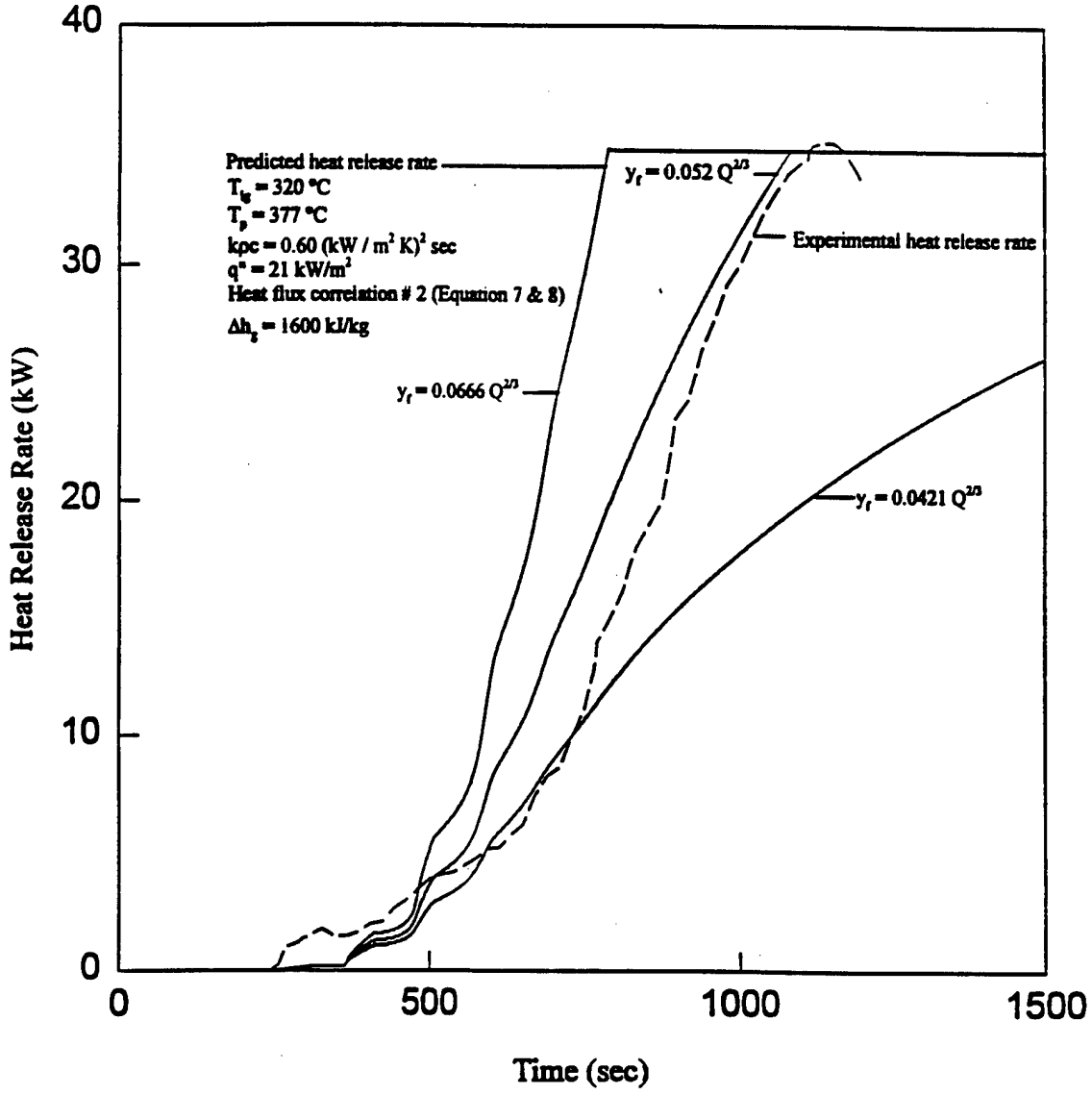

Figure 22 Comparison of heat release rate predictions for a 0.90 m x 0.20 m vertical PMMA surface different flame height correlation with Wu, Delichatsios, and de Ris, 1993 data (reference (11))

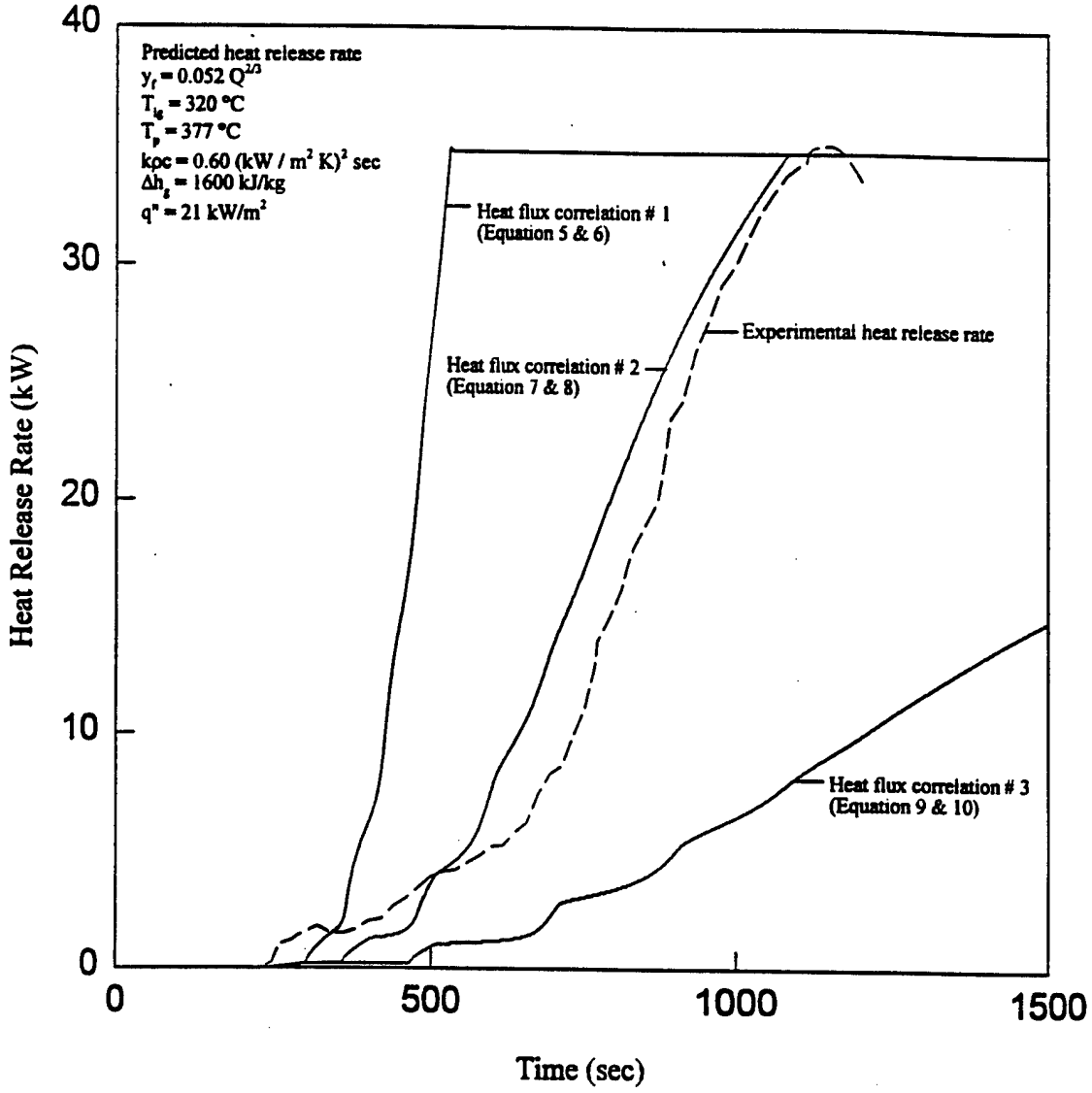

Figure 23 Comparison of heat release rate predictions for a 0.90 m x 0.20 m vertical PMMA surface different heat flux correlations with Wu, Delichatsios, and de Ris, 1993 data (reference (11))

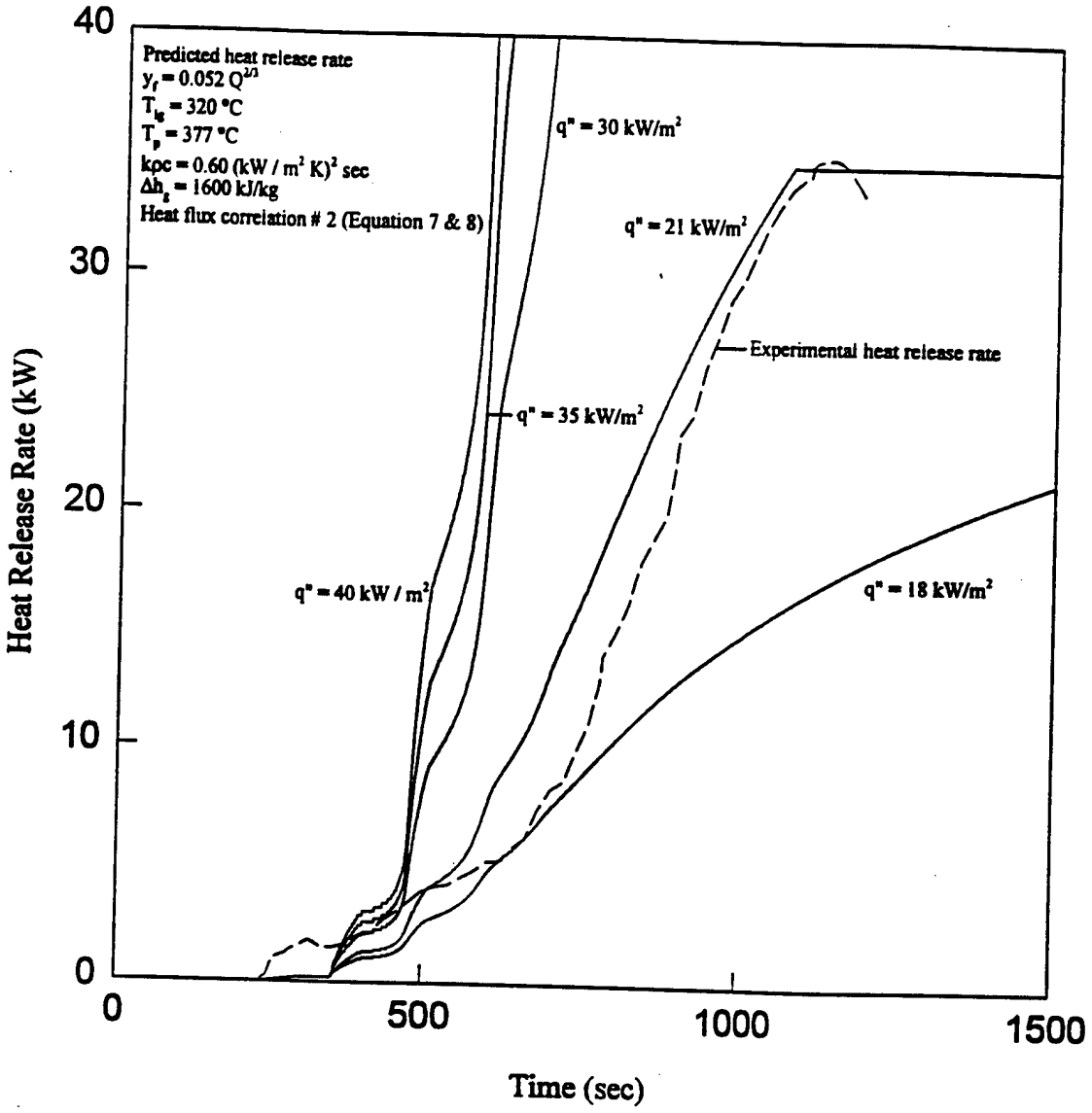

Figure 24 Comparison of heat release rate predictions for a 0.90 m x 0.20 m vertical PMMA surface different values of heat flux after ignition with Wu, Delichatsios, and de Ris, 1993 data .(reference (11))

The effect of variations in the heat flux to the wall during burning are illustrated in Fig. 23. The range of heat fluxes examined in the Figure corresponds to the range of experimental data available in the literature. As the Figure indicates, the variations in heat release rate are very significant. This also indicates that additional work in the measurement and correlation of heat fluxes to walls is needed. The level of certainty represented by the literature is simply not sufficient to support accurate predictions.

The effect of heat flux to the already burning surface is shown in Figure 24. The range of fluxes shown in the Figure represents the range of values reported in the literature. Clearly, the behavior of the material is critically impacted by the heat flux to the burning material. The results are particularly sensitive to the heat flux for lower heat fluxes where spread rates are slow and indefinite flame spread is not expected. It is known that the heat flux to the burning surface is scale dependent with larger fluxes associated with taller wall flames. However, the details of the scale effects are not sufficiently well known to allow their inclusion in the model. Additional work in this area is needed.

4.6 Discussion of the Sensitivity Analysis

The inputs assessed in the prior section can be classified generally as material properties inputs and wall heat transfer inputs. It can be hypothesized that the wall heat transfer inputs are only modestly dependent on the fire properties of the material, though the luminosity of the flame is clearly dependent on the nature of the fuel volatiles. The range of wall heat transfer inputs examined in the prior section generally reflects the range of results available in the research literature at this time. While the use of average values for these inputs were generally quite successfully used for data comparisons in Sections 4.2, 4.3, and 4.4, the sensitivity analysis indicates that improved precision in these inputs is needed to support accurate predictions of flame spread and resulting heat release rate. The need for accurate inputs is particularly keen under conditions were acceleratory flame spread is not present or where it is marginally present. Since a major goal of these models is to assess materials to allow selection of materials which do not support acceleratory flame spread, this need for increased precision is critically important for practical use of the model and is in no sense academic. This points to the need for well controlled experimental work in this area.

The material properties inputs are equally critical to the performance of the model. As Section 4.4 indicates, the poorest predictions of material performance were for experimental conditions where acceleratory flame spread did not occur for the wood particleboard. While it was anticipated that the relatively simple solid phase material response models used would be sufficiently accurate to allow good predictions of material behavior, it is clear at this point that more detailed models will be required to reproduce actual material fire performance. The ignition model seems to be fully adequate at this time. However, the burning rate model used here needs to be further developed to achieve the required accuracy. The pyrolysis temperature assumed to be constant in this model can vary enough to seriously compromise the results for materials like wood. Further, the heat of gasification model also needs improvement to achieve the desired level of accuracy.

The difficulties with using a more sophisticated model of the solid phase response of the burning material are two-fold. First, as the models are made more sophisticated, they also become less general. This means that there may need to be multiple models applicable to different material types. For instance a separate model may be required for charring and non-charring materials or thick and thin fuels. This is an obvious difficulty in that the ease of use of the model can quickly be degraded. The second difficulty is the increased data requirements of more sophisticated models. Ultimately, this concern is greater than the model generality concern. As more inputs are required, the number and detail of the bench scale tests needed increases. This would ultimately require many more tests and require the cone calorimeter instrumentation to be developed to a much higher level than is currently used. In terms of the ultimate use of the model, the demands on the number and sophistication of the bench scale tests required are the most serious concern.

While the foregoing discussion focuses on the uncertainties and limitations of the present model, the comparisons shown in Sections 4.2, 4.3, and 4.4 are very good indeed. The use of the best available inputs and parameters has been shown to result in very credible predictions. Thus, we have direct evidence of the value of the modeling approach adopted here and the prospects for a valuable material assessment tool.

5.0 PREDICTION OF VERTICAL FLAME PROPAGATION OVER THERMALLY THIN MATERIAL ON NON-COMBUSTIBLE SUBSTRATES

5.1 Introduction

The goal of the flame spread model is to provide a link between bench scale test results and full scale fire performance. The current model has only been developed to date to include upward flame spread on vertical surfaces. Preliminary work to generalize this model is described in Section 5.4. However, the development of the model and the room corner fire testing performed onboard the ex-USS SHADWELL (reference (26)) using the U.S Navy material test program has motivated a simple method for correlating bench-scale fire test results with full scale corner fire test results. The correlational method described here was developed previously and reported in NRL Letter Report (reference (27)) and is included here for completeness.

The flame spread performance of U.S. Navy materials,. Williams, et al. (reference (28)) , (Glass Reinforced Plastic Nomex Panel, Manville Thermal Insulation, Imi-Tech Acoustic Insulation, and Waffle-Board Acoustic Insulation) have been evaluated and compared with the flame spread test results on textile wall covering materials on non-combustible substrates (Harkleroad, reference (29)). The Navy cone calorimeter tests (reference (28)) were conducted by the Carderock Division, Naval Surface Warfare Center (NSWC/CD) Code 643, and full-scale calorimeter tests were conducted aboard ex-USS SHADWELL (LSD-15).

In the next section, the flame spread model is presented to provide the theoretical basis for the flammability parameter developed by Mowrer and Williamson (reference (25)).

5.2 Formation of Flame Spread Parameter

The flame spread model developed by Mowrer and Williamson (reference (25)) is based on the approach presented by Quintiere, Harkleroad and Hasemi (reference (30)) for the prediction of upward flame spread over materials. The upward flame spread model (reference (25)) includes consideration of the finite burning time t_b of thin fuels. The consumption of the wall fuel results in burnout of the flame at that location, which is an important aspect of flame spread on thin fuels.

In this model, the flame spread rate is defined as the rate of pyrolysis front advance:

$$V_p = \frac{dy_p}{dt} \approx \frac{y_p(t + t_f) - y_p(t)}{t_f} = \frac{y_f(t) - y_p(t)}{t_f} \tag{25}$$

where V_p is the upward spread velocity (m/s), y_p is the height of the pyrolysis front (m), t is time (s), t_f is the flame spread time (s), and y_f is the flame height (m). The characteristic flame spread (or ignition) time is defined in terms of a simple thermal model of heating a wall with constant thermal properties

$$t_f \approx k\rho c \left(\frac{(T_{ig} - T_s)}{\dot{q}''_{net}} \right)^2 \tag{26}$$

where all terms have been previously defined. Once burnout begins, the velocity of the burnout front can be expressed as:

$$V_b = \frac{dy_b}{dt} \approx \frac{y_b(t + t_{bo}) - y_b(t)}{t_b} = \frac{y_p(t) - y_b(t)}{t_{bo}} \tag{27}$$

where V_b is the upward velocity of the burnout front, t_{bo} is the burning duration(s), t_b is the burnout time(s), and y_b is the burnout front height (m).

A linear flame height approximation is used to describe the flame height required in Equation (1), following Saito, Quintiere, and Williams (reference (13)), Quintiere, Harkleroad, and Hasemi (reference (30)), and Cleary and Quintiere (reference (31)). Before burnout begins, this flame height approximation can be expressed as follows:

$$\frac{y_f}{y_p} = k_f \dot{E}'' \tag{28}$$

After burnout begins, the dimensionless flame height is expressed as follows:

$$\frac{(y_f - y_b)}{(y_p - y_b)} = k_f \dot{E}'' \tag{29}$$

The parameter k_f is a correlating factor used to define the flame length. Cleary and Quintiere (reference (31)) suggest a value of approximately 0.01 m^2/kW, for k_f. Using Equation (28) for times $t < t_b$, Equation (25) can be rewritten as follows:

$$\frac{dy_p}{dt} = (k_f \dot{E}'' - 1) \frac{y_p}{t_f} \tag{30}$$

Equation (30) can be integrated, with the limit that $y = y_{po}$ at $t = 0$ and $y = y_p$ at t:

$$y_p = y_{po} \exp\left(\frac{(k_f \dot{E}'' - 1)\, t}{t_f}\right) \tag{31}$$

Equations (30) and (31), together with Equation (28), suggest that, before burnout, the flame spread rate will accelerate if $y_f > y_p$ and decelerate if $y_f < y_p$, i.e., if $k_f \dot{E}'' < 1$. After burnout begins, at times $t > t_b$, the net rate of flame propagation can be expressed as the difference of the pyrolysis front velocity and the burnout front velocity:

$$V_p(t) - V_b(t) = \frac{d}{dt}(y_p - y_b) = \frac{(y_f - y_p)}{t_f} - \frac{(y_p - y_b)}{t_{bo}} \tag{32}$$

Using Equation (29), Equation (32) can be rearranged to the following:

$$\frac{d}{dt}(y_p - y_b) = (y_p - y_b)\left(\frac{(k_f \dot{E}'' - 1)\, t_{bo} - t_f}{t_f\, t_{bo}}\right) \tag{33}$$

Equation (33) can then be integrated, with the limit of $(y_p - y_b) = (y_{pl} - y_{po})$ at $t = t_b$ and $(y_p - y_b) = (y_p - y_b)$ at time t, to yield the pyrolysis zone height:

$$(y_p - y_b) = (y_{pl} - y_{po}) \exp\left(k_f \dot{E}'' - \frac{t_f}{t_{bo}} - 1\right)\left(\frac{t - t_b}{t_f}\right) \tag{34}$$

Equation (34) suggests that, following the onset of fuel burnout, the potential for accelerating flame spread depends on a balance among three parameters: the normalized flame height, $(y_f - y_b) / (y_p - y_b)$, which is represented per Equation (29) as a linear function of unit heat release rate , $\dot{E}$; the flame spread time, t_f, given by Equation (26); and the burning duration, t_{bo}. If the parameter $(k_f \dot{E}'' - t_f / t_b) > 1$, the predicted flame spread will accelerate. The flammability parameter is thus defined as $\dot{E}'' k_f - t_f / t_b$. While this model is based on several idealizations, it is expected that this flammability parameter characterizes a material with regard to vertical flame spread. However, attention must be paid to the methods used to evaluate $\dot{E}''$, t_f, and t_b. Mowrer and Williamson evaluated $\dot{E}''$ as the peak heat release rate of the material, t_f as the ignition time, and t_b as the time from ignition to the peak heat release rate. They evaluated these quantities at both cone calorimeter heat fluxes (30 and 50 kW/m^2) tested by Harkleroad (reference (29)). Based on their results, the correlation was better using the cone data at 50 kW/m^2.

There are problems with the methods proposed by Mowrer and Williamson for deducing $\dot{E}''$ and t_b from cone calorimeter data. The problems are unique to thin materials which have burn times less than approximately a minute. The time response characteristics of the cone calorimeter are such that the peak measured heat release rate is less than the actual peak for these thin materials due to the small burn time. The effect of various burning durations can be seen from Fig. 25 for a methane burner at a heat release rate of 6.80 kW operated for various durations. Of course, if the cone had a zero response time, the measured heat release rates would be square wave pulses with the width equal to the burning duration. For the longer burning

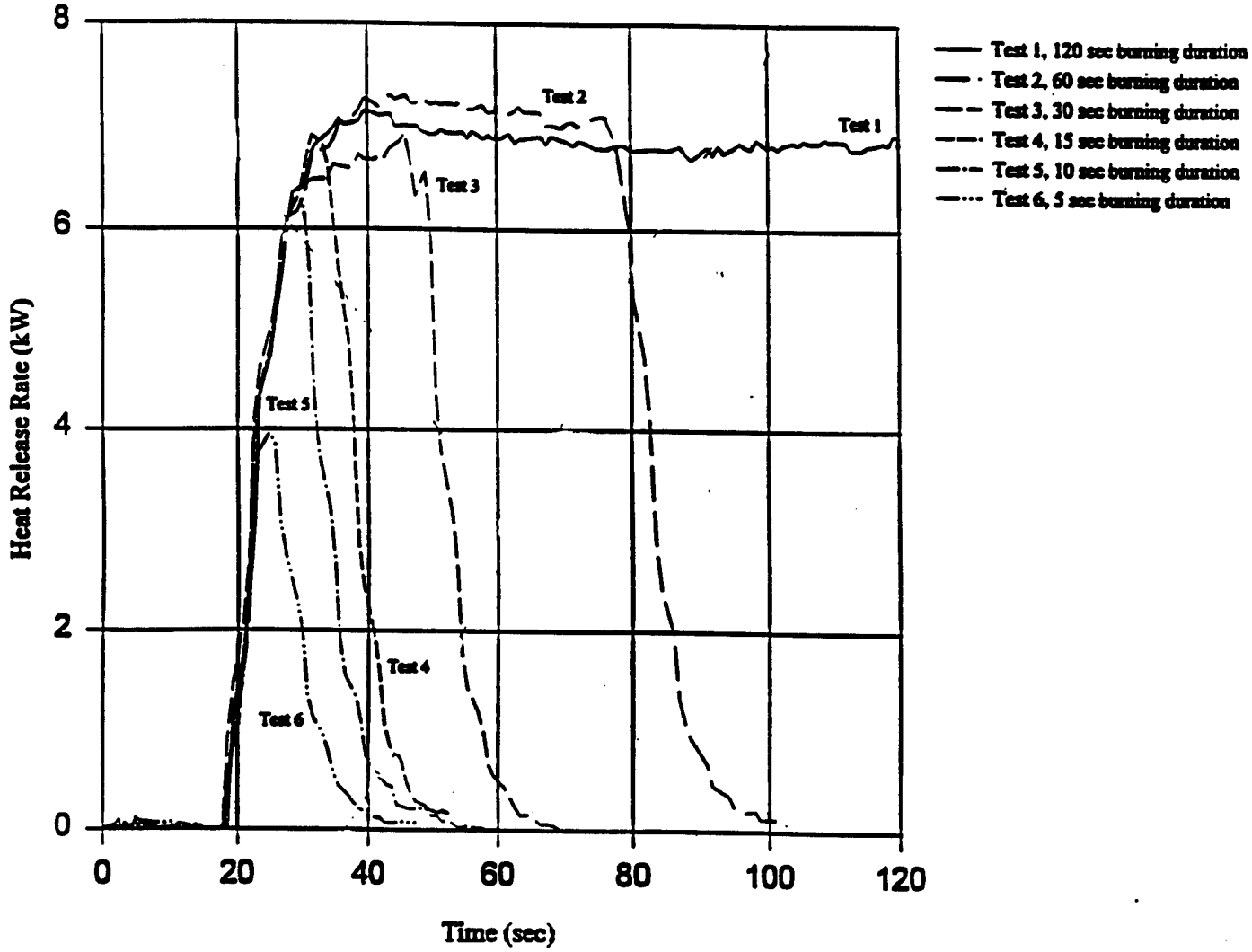

Figure 25 Heat release rate for methane burner operated at 6.80 kW steady state

durations (test 1, 120 sec burn duration) the actual heat release rate is measured after about 10 seconds. For shorter burn durations (test 5, 10 sec and test 6, 5 sec), the peak recorded heat release rate occurs at about 5-10 seconds, and the actual burning rate is never recorded. While the response time of the gas analysis system on the cone calorimeter does not allow correct measurement of the heat release rate, there is hope that the cumulative heat release may be measured correctly despite the time response limitations of the system. The cumulative heat release is the area under the heat release rate verses time curve. Table 8 shows the predicted and measured cumulative heat releases for the various burn durations. The results indicate that the cone calorimeter can correctly measure the cumulative heat release for short duration burns.

Table 8. Measured and Predicted Cumulative Rate of Heat Release for a Methane Burner Operated at 6.8 kW

Test number	Test duration (sec)	Measured cumulative heat release rate (kJ)	Predicted cumulative heat release rate (kJ)
1	120	830.73	816
2	60	429.81	408
3	30	204.89	204
4	15	109.47	102
5	10	77.75	68
6	5	36.70	34

There are also problems with the burn time used by Mowrer and Williamson, which is taken as the time from ignition to the time of the peak rate of heat release rate. There are several problems with this method. The first is the significant effect of response time on the measured time to peak heat release. This is directly related to the peak heat release measurement concern and is particularly acute since peak heat release rates typically occur shortly after ignition. Second, if the peak heat release occurs soon after ignition and significant heat release occurs after the peak, the actual heat output duration may not be well represented by the Mowrer and Williamson definition of burn time. Typically, thick and thin coverings of the same material would have the same burn time as determined by the Mowrer and Williamson method whereas their observed burning durations would be very different.

In order to address these problems, new methods of cone calorimeter data reduction have been studied, and a modified method has been developed. The burn time, t_b, is taken as the time from ignition until the material stops flaming. This is best determined visually, but can be determined from the heat release rate verses time output from the cone calorimeter. For all materials examined by Harkleroad (reference (29)), burn times were determined from the cone calorimeter heat release rate data. For the Navy materials tested, the burn time was determined from visual observation during the cone calorimeter test. The heat release rate, $\dot{E}''$, is taken as the cumulative heat release as routinely determined in the cone calorimeter divided by the burn time, t_b. This is an average heat release rate for the material during the active burning period. These modified methods avoid some of the experimental difficulties with the cone calorimeter as applied to thin materials.

5.3 Experimental Data and Implication of the Model

The flammability parameter derived from cone calorimeter test results for the 50 kW/m^2 heat flux exposure for nine textile wall covering materials on gypsum board are tabulated in Table 9 along with the peak heat release rates measured in the large-scale corner tests performed by Fisher, MacCraken, and Williamson (reference (32)) at the University of California, Berkeley. The flammability parameter from cone calorimeter test results for the four passive fire protection (PFP) Navy materials are tabulated in Table 10 for 50 kW/m^2 heat flux exposure to the specimen surface along with the peak heat release rates measured in the full-scale corner tests performed on the ex-USS SHADWELL. The correlation of the peak full-scale heat release with the flammability parameter from data for the 50 kW/m^2 exposure level for each of the Navy materials and the nine textile wall covering materials on gypsum board are shown in Fig. 26. Fig. 26 shows that the correlation of the full-scale results by the flammability parameter is quite good. Based on the performance required in full-scale applications, Fig. 26 could be used to establish the required value of the flammability parameter for inclusion in material specifications for that application.

Table 9. Summary of Flammability Parameter for Textile Wall Covering Materials on Gypsum Board 50 kW/m^2 Incident Heat Flux Exposure (reference (29), (31))

Textile wall covering* fabric	Heat release rate from full-scale fire test (kW)**	Avg. heat release rate (bench-scale) $\dot{E}''$ (kW/m^2)	Flame length parameter k_f (m^2/kW)	Flame spread time t_f (s)	Burnout time t_b (s)	Flammability parameter = $[\dot{E}''k_f - t_f/t_b]$
B	207 (298)	125	0.01	34	46	0.51
Q	207 (497)	130	0.01	33	37	0.41
Q-FR	310	117	0.01	33	57	0.59
G	83	37	0.01	19	31	-0.23
C2	62 (119)	70	0.01	34	36	-0.24
H	46 (160)	56.5	0.01	20	45	0.12
AA	684	185	0.01	16	140	1.73
R	587 (590)	145	0.01	25	60	1.03
C1	--	70	0.01	25	45	0.14
PP-PF	(1166)	131	0.01	25	85	1.01

* - See Fig. 26 for description.

** - Parenthetical peak heat release rates are for two foot wide samples while normal values are for one foot wide samples.

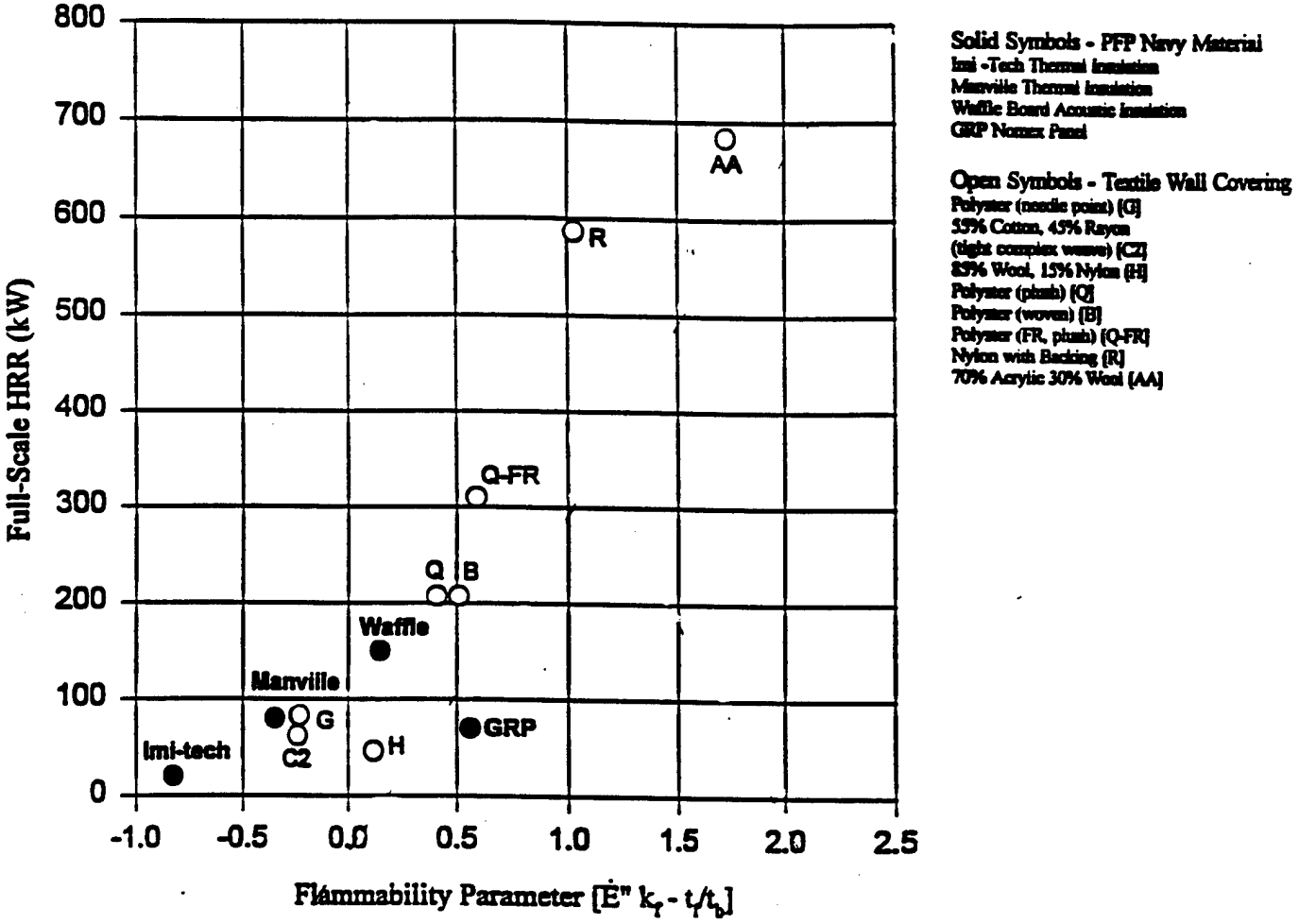

Fig. 26 Comparison of Navy results with textile wall covering on gypsum board results (Harkleroad, 1989, reference (29) and Fisher et al. 1986 (reference (32))

Table 10. Summary of Flammability Parameter for the PFP Navy Test Materials, 50 kW/m^2 Incident Heat Flux Exposure (reference (28))

PFP Navy test material	Heat release rate from full-scale fire test (kW)	Avg. heat release rate (bench-scale) $\dot{E}''$ (kW/m^2)	Flame length parameter k_f (m^2/kW)	Flame spread time t_f (s)	Burnout time t_b (s)	Flammability Parameter = $[\dot{E}''k_f - t_f/t_b]$
GRP Nomex panel	70	68	0.01	14	120	0.56
Manville thermal insulation	80	5	0.01	8	20	-0.35
Imi-tech acoustic insulation	20	7.5	0.01	9	10	-0.82
Waffle board acoustic insulation	150	60	0.01	9	20	0.15

If one examines Fig. 26, the GRP data point appears to be somewhat of an outlier. Based on the flammability parameter of 0.56, one would have expected a higher full-scale heat release rate. This material burns vigorously where the surface is breached by cracking due to heating. This behavior is emphasized in the cone calorimeter in that such a crack always occurred in the small sample while cracking occurred at a relatively wider spacial separation in the full-scale test. Thus, the cone calorimeter test results are worse than expected in full-scale. Such scaling problems must be expected to occur for some materials in a small-scale test and is an inherent limitation of small-scale testing. However, the effect is not significant for any of the materials tested in this program.

A flammability parameter based on concurrent vertical flame spread modeling has been developed to allow correlation of bench-scale ignition and heat release rate measurements in the cone calorimeter with full-scale fire performance. The cone calorimeter data, at an exposure level of 50 kW/m^2 for both Navy insulation materials and the textile wall coverings on gypsum board shown in Figure 26, demonstrate the general trend that materials with low heat release in full-scale fire tests have low flammability parameter values, and materials with high heat release rate in real-scale fire tests have high values of the flammability parameter. As expected, the behavior of materials change at a flammability parameter of about one. The correlation successfully links cone calorimeter results to full-scale fire performance for Navy wall covering material, which allows specifications to be developed which will result in known fire behavior in full-scale applications.

5.4 Generalization of the Current Upward Flame Spread Model

The computer model developed to predict upward flame spread and burning of a wall has been designed to be generalized to allow modeling a fire against a wall as well as to predict corner fire scenarios. This requires the implementation of additional heat transfer modeling involving the new fire source as well as wall to wall heat transfer.

6.0 CONCLUSIONS

A computer model has been developed that successfully addresses upward fire growth on vertical surfaces. The agreement with experimental results is good. Assumptions have been made based on the limited information for flame heat transfer rates to cause burning and spread, and more complete experimental results are needed. Small variations in the material properties, flame height correlation, and flame heat flux after ignition can have a significant effect on fire growth. Variations in ignition and flame spread properties affect the predictions significantly as well. Therefore, material properties must be accurately determined to predict the flame spread characteristics of the material. Despite the sensitivity of the model to many input parameters, the model demonstrated good results over a range of experimental conditions.

The predicted heat release rates for PMMA in both the small and full-scale wall fires are in good agreement with the data using two different flame height correlations. The use of two flame height correlations in the model is due to the absence of side walls in the experiments conducted in reference (11), heat flux distribution, and/or width effects.

Approximate wall heat flux profiles have been developed based on the steady-state experimental data available in the literature (refer Figure 3). There is considerable scatter and/or uncertainty in the data above the pyrolysis zone for burning wall material. The fluxes in the flame region have been measured in the range of 20-40 kW/m^2 and fall rapidly at $y > y_f$. Additional work is required to improve correlations of these heat fluxes.

The properties of the materials used in the model are either directly found from the literature or deduced from bench-scale experimental data. Further work in the modeling and measurement of solid phase response of materials to heat is required to improve prediction capability.

It is the intent of this work to present a simple flame spread model that integrates many of the features and capabilities of those described, that requires a minimum of input data and which accurately predicts the fire growth along vertical walls subject to ignition sources. Currently, it is generalized with respect to the wall material. Ultimately, the model will be generalized so that a number of two and three dimensional geometries may be modeled.

The ultimate goal of these modeling efforts to predict and evaluate the fire performance of U. S. Navy materials, products, and assemblies and to provide a link between bench-scale ignition and heat release rate measurements in the cone calorimeter with full-scale fire performance to ensure an environment safe from destructive fires for the Navy requirements. To achieve this goal, this model will be used to predict fire performance of the Navy materials, and allow specifications to be developed which will result in known fire behavior in full-scale applications.

The work has developed a correlational method which relates bench-scale fire test results to full-scale corner fire test results. Further development of the model will broaden our capabilities to correlate bench- and full-scale results. Ultimately, a full predictive link between bench- and full-scale can be developed through development of this model.

7.0 REFERENCES

1. Beyler, C. L., and Williams, F. W., 1994, "Passive Fire Protection (PFP) Modeling Literature Review," NRL Ltr Rpt Ser 6180/0221A, 13 July 1994.

2. ASTM E 1354-92, "Standard Test Method for Heat and Visible Smoke Release Rates for Materials and Products Using an Oxygen Consumption Calorimeter," *ASTM Fire Test Standards*, Fourth Edition, American Society for Testing and Materials, Philadelphia, PA, 1993, pp. 968-984.

3. Quintiere, J. G., and Cleary, T. G., "Heat Flux from Flames to Vertical Surfaces," *Fire Technology*, **30** (2), 1994, pp. 209-231.

4. Delichatsios, M. A., "Flame Heights in Turbulent Wall Fires with Significant Flame Radiation," *Combustion Science and Technology*, **39**, 1984, pp. 195-214.

5. Tu, K-M., and Quintiere, J. G., "Wall Flame Heights with External Radiation," *Fire Technology*, **27** (3), August 1991, pp. 195-203.

6. Tewarson, A., 1995 in *The SFPE Handbook of Fire Protection Engineering*, DiNenno, Editor, Second Edition, National Fire Protection Association, Quincy, MA, 1995 (in publication).

7. Quintiere, J. G., "The Application of Flame Spread Theory to Predict Material Performance," *Journal of Research of the National Bureau of Standards*, **93** (1), January/February 1988, pp. 61-70.

8. Mitler, H. E., "Predicting the Spread Rates of Fires on Vertical Surfaces," *Twenty-third International Symposium on Combustion*, The Combustion Institute, Pittsburgh, PA, 1990, pp. 1715-1721.

9. Eckert, E. R., and Drake, R. M., *Analysis of Heat and Mass Transfer*, Chapter 4 - Unsteady Heat Conduction, McGraw-Hill Book Company, 1972, pp. 138-221.

10. Quintiere, J. G., and Harkleroad, M. T., "New Concepts for Measuring Flame Spread Properties," *Fire Safety Science and Engineering, ASTM STP 882*, Harmathy, Editor, American Society for Tasting and Materials, Philadelphia, 1985, pp. 239-267.

11. Wu, P-K, Delichatsios, M. M., and de Ris, J., "Upward Fire Spread Over PMMA Walls-A Model/Experiment Comparison," *1993 Annual Conference on Fire Research: Book of Abstracts*, NISTIR - 5280, U.S. National Institute of Standard and Technology, Gaithersburg, MD, 1993, pp. 7-10.

12. Delichatsios, M. M., Wu, P-K., Delichatsios, M. A., Lougheed, G. H., Crampton, G. P., Qian, C., Ishida, H., and Satio, K., "Effects of External Radiant Heat Flux on Upward Fire Spread: Measurements on Plywood and Numerical Predications," *Fire Safety Science-Proceedings of the Fourth International Symposium*, International Association of Fire Safety Science, 1994, pp. 421-432.

13. Saito, K., Quintiere, J. G., and Williams, F. A., "Upward Turbulent Flame Spread," *Fire Safety Science-Proceedings of the First International Symposium*, International Association of Fire Safety Science, Hemisphere Publishing Corporation, 1987, pp. 75-86.

14. Takashi, K., and Ohlemiller, "A Steady of Oxygen Effects on Nonflaming Transient Gasification of PMMA and PE During Thermal Irradiation," *Proceedings of the Nineteenth International Symposium on Combustion*, The Combustion Institute, Pittsburgh, PA, 1982, pp. 815-823.

15. Tewarson A, and Pion, R. F., "Flammability of Plastics-I. Burning Intensity," *Combustion and Flame*, **26**, 1976, pp. 85-103.

16. Jackson, J. L., "Direct Measurement of Heat of Gasification for Polymethylmethacrylate," NISTIR 88-3809, U.S. National Institute of Standard and Technology, Gaithersburg, MD, October 1988.

17. Agrawal, S., and Atreya, A., "Wind-Aided Flame Spread Over an Unsteadily Vaporizing Solid," *Proceeding of the Twenty-fourth International Symposium on Combustion*, The Combustion Institute, Pittsburgh, PA, 1992, pp. 1693-1885.

18. Tewarson, A., and Ogden, S. D., "Fire Behavior of Polymethylmetacrylate," *Combustion and Flame*, **89**, 1992, pp. 237-259.

19. Tewarson, A., "Flammability Parameters of Materials: Ignition, Combustion, and Flame Spread," *Proceedings of the International Conference for the Promotion of Advanced Fire Resistant Aircraft Interior Materials*, February 9-11, 1993, pp. 263-281.

20. Delichatsios, M. A., Panagiotou, T. H., and Kiely, F., "The Use of Time to Ignition Data for Characterizing the Thermal Inertia and the Minimum (Critical) Heat Flux for Ignition or Pyrolysis," *Combustion and Flame*, **84**, 1991, pp. 323-332.

21. Orloff, L., de Ris, J., and Markstein, G. H., "Burning of Large Scale Vertical Surfaces," *Fifteenth International Symposium on Combustion*, The Combustion Institute, Pittsburgh, PA, 1974, pp. 183-192.

22. Janssens, M. L., "Fundamental Thermophysical Characteristics of Wood and their Role in Enclosure Fire Growth," Doctor of Philosophy Dissertation, University of Gent, Belgium, September 1991.

23. Parker, W. J., "Prediction of the Heat Release Rate from Basic Measurements," *Heat Release in Fires*, Babrauskas and Grayson, Editors, Elsevier Applied Science, 1992, pp. 333-356.

24. Atreya, A., "Pyrolysis, Ignition and Fire Spread on Horizontal Surface of Wood," Doctor of Philosophy Dissertation, Harvard University, Cambridge, MA, May 1983.

25. Mowrer, F. W., and Williamson, R. B., "Flame Spread Evaluation for Thin Interior Finish Materials," *Fire Safety Science-Proceedings of the Third International Symposium*, International Association of Fire Safety Science, Cox and Langford, Editor, 1991, pp. 689-698.

26. Williams, F. W. Toomey, T. A. And Carhart, H. W., "The ex-USS SHADWELL Full-Scale Fire Research and Test Ship," NRL Memorandum Report 6074, revised January 20, 1988, reissued 1992.

27. Williams, F.W., Beyler, C. L., and Iqbal, N., "Flame Spread Evaluation for the U.S. Navy Passive Fire Protection (PFP) Test Materials," NRL Ltr Rpt Ser 6180/0216.2, April 25 1995.

28. Williams, F. W., Havlovick, B. J., Beitel, J. J., Gottuk, D. T., and Peatross, M. J., "Initial Cone Calorimeter and Real-Scale Single Compartment Fire Test," NRL Ltr Rpt Ser 6180/0026.2, 23 March 1994.

29. Harkleroad, M. F., "Fire Properties Database for Textile Wall Coverings," NISTIR 89-4065, National Institute of Standard and Technology, Gaithersburg, MD, March 1989.

30. Quintiere, J. G., Harkleroad, M., and Hesemi, Y, "Wall Flames and Implications for Upward Flame Spread," *Combustion Science and Technology*, **48**, 1986, pp. 191-222.

31. Clearly, T. G., and Quintiere, J. G., "A Framework for Utilizing Fire Properties Tests," *Fire Safety Science-Proceeding of the Third International Symposium*, International Association of Fire Safety Science, Cox and Langford, Editors, 1991, pp. 647-656.

32. Fisher, F. L., MacCraken, W., and Williamson, R. B., "Room Fire Experiments of Textile Wall Coverings-A Final Report of All Materials Tested Between March 1985 and January 1986," ES-7853, Service to Industry Report No. 86-2, Fire Research Laboratory, University of California Berkeley, CA, March 1986.

Appendix A

Input Data

Integer 1 - 7: Version control flag (current version requires a 7 to run
The version number parameter specifies the version of flame spread model for which the input file was prepared. This prevent different input formate to be used.

Integer 0 or 1: Burner control flag 0 - normal 1 - never shut off
0 specifies that the ignition source is turned off where all material behind flame is consumed. 1 indicates that burner remains on. Only used for line burner exposures.

Integer 0 or 1: Debug on/off 0 - off 1 - on
Debug on prints various values and diagnosed messages to several files and send additional data to the screen.

Integer 1 - 4: Analysis type
There are several analysis flags available in the model. There can be a line fire source across the entire lower length of the wall, or line fire source across some specific length of a wall, and or pool fire exposure adjacent to the wall. 1 - Line burner, 2 - Partial line burner, 3 - Pool fire, and 4 - Pool fire in corner.

Integer 0 or 1: Cone calorimeter test 1 - true 0 - false
Cone test exposure has no ignition source and has a uniform flux over the surface area.

Real > 0: Height: Height specifies the height of the vertical sample in meters
Real > 0: Width: Width specifies the width of the vertical sample in meters
Real > 0: Thickness: Thickness specifies the thickness of the sample in meters

Integer: Number of nodes in the horizontal direction **Integer: Number of nodes in the vertical direction**
Computer model calculates the flame spread on the vertical sample by breaking up the surface into a large number of elements and each element is bounded by four nodes.

Real: Thermal inertia (kpc) $(kW/m^2 K)^2$ sec
The thermophysical property of the vertical surface from open literature.

Real: Ignition temperature, K
Ignition temperature of the material from open literature.

Real: Heat of combustion (kJ/kg)
Heat of combustion of the material from open literature.

Real 0 - 1: Fractional of mass consumed
Specifies a fraction of mass/area that is involved in the burning process. This may represent char or non-combustible constituents.

Real > 0: Density, kg/m^3
Density of the material from open literature.

Real: Pyrolysis temperature, K
Available in the open literature.

Real: Ambient temperature, K
Ambient temperature is the temperature of the ambient atmosphere.

Real: Initial temperature, K
Typically, the initial temperature is the same as ambient temperature, but in some cases, for the ignition simulation the sample is preheated at preset temperature from external radiation source, then the initial temperature is different from ambient temperature.

Integer 1 - 4: Fire type (flame height correlation)
Flame height correlation for a line fire against a wall or wall fire described in Section 2.2.

Real > 0: Imposed heat flux (kW/m^2)
External heat flux from a radiant panel or cone heater.

Real > 0: Flame heat flux after ignition (kW/m^2)
Experimentally determined incident heat flux from wall flames to the surface described in the Section 2.2.

Real > 0: Temperature difference, K
Specifies temperature rise of material above initial temperature where the surface temperature calculations switches from Scant method to Runge-Kutta method. Usually 0.5 to 1.0 K.

Integer 1 - 4: Flem heat flux correlation
Upon the ignition of the wall, the luminosity of the flame may increase over a typical of methane ignitor flame. To allow for this, the model allows the use of different heat flux correlation after ignition of the wall as described in Section 2.2.

Real > 0: Peak heat flux, used only with flame heat flux correlation # 4
The experimental peak heat flux from flame of burning material.

Integer 0 - 2: 0 - do not use special line fir e fluxes, 1, 2 - use high and low respectively.
1 or 2 specified that a material heat flux exposure be used for the line burner.

Real: Convection factor (W/m^2-K)
The convection factor used when calculating heat loss from cone test analysis.

Real 0 - 1: Emissivity/Absorptivity of the material surface
Radiative emissivity/Absorptivity of material, used for computing heat loss without gain.

Real > 1: This is the minimum ratio between the fire height and the pyrolysis height
This presents the flame height from falling below the pyrolysis height for low heat release rate materials.

Real > 0: Time max, sec
The time is the length of time over which the simulation takes place.

Real > 0 < Time max: Calculation interval, sec
The calculation interval is the time interval between each writing of the output to the final results of the simulation.

Real > 0: HRR/unit length, kW/m
Line burner strength.

Real ≥ 0: Time to burner to rise, sec
Allows line burner to rise from 0 to final value over a finite time.

Integer ≥ 0: Number of voids
Any air gaps or inert material on a vertical surface left, represented by voids.

A - 1 - Input data: Small-scale PMMA

7	Version control flag (current version requires a 1 to run)
0	Burner control flag 0 - normal 1 - never shut off
0	Debug on
1	Analysis type
0	Cone Calorimeter test 1 - true 0 - false
0.90	Height (m)
0.20	Width (m)
0.0254	Thickness (m)
2	Number of nodes in the horizontal direction
500	Number of nodes in the vertical direction
0.60	Thermal inertia (kρc) $(kW/m^2\ K)^2$ sec
593.0	Ignition temperature (T_{ig}) (K)
25000.0	Heat of combustion (kJ/kg)
1.00	Percent of the mass burned of (1- this is what remains)
1200.0	Density (kg/m^3)
650.0	Pyrolysis temperature (K)
298.0	Ambient temperature (K)
298.0	Initial Temperature (K)
2	Fire type (Flame height correlation)
0.0	Imposed flux (kW/m^2)
21.0	Flame flux after ignition (kW/m^2)
2.0	Temperature difference (°C or K)
2	Flame heat flux correlation
0.0	Used only with flame heat flux correlation # 4
0	0 - do not use special line fire fluxes, 1, 2 - use forms
0	Convection factor (W/m^2-K)
0.9	Emissivity/Absorptivity of the material surface
1.1	This is the minimum ratio between the fire height and the pyrolysis height
1500	Time max (sec)
1.0	Calculation interval (sec)
1.0	HRR/unit length (kW/m)
60.0	Time to burner to rise (sec)
0	Number of voids

A - 2 Input data: Full-scale PMMA

7	Version control flag (current version requires a 1 to run)
0	Burner control flag 0 - normal 1 - never shut off
0	Debug on
1	Analysis type
0	Cone Calorimeter test 1 - true 0 - false
5.0	Height (m)
0.58	Width (m)
0.0254	Thickness (m)
2	Number of nodes in the horizontal direction
500	Number of nodes in the vertical direction
0.60	Thermal inertia (kρc) $(kW/m^2\ K)^2$ sec
593.0	Ignition temperature (T_{ig}) (K)
25000.0	Heat of combustion (kJ/kg)
1.00	Percent of the mass burned of (1- this is what remains)
1200.0	Density (kg/m^3)
650.0	Pyrolysis temperature (K)
298.0	Ambient temperature (K)
298.0	Initial Temperature (K)
3	Fire type (Flame height correlation)
0.0	Imposed flux (kW/m^2)
31.0	Flame flux after ignition (kW/m^2)
2.0	Temperature difference (°C or K)
2	Flame heat flux correlation
0.0	Used only with flame heat flux correlation # 4
0	0 - do not use special line fire fluxes, 1, 2 - use forms
0	Convection factor (W/m^2-K)
0.9	Emissivity/Absorptivity of the material surface
1.1	This is the minimum ratio between the fire height and the pyrolysis height
1500	Time max (sec)
1.0	Calculation interval (sec)
1.0	HRR/unit length (kW/m)
60.0	Time to burner to rise (sec)
0	Number of voids

A - 3 Input data: Full-scale Plywood (Test # 1)

7	Version control flag (current version requires a 1 to run)		
0	Burner control flag	0 - normal	1 - never shut off
0	Debug on		
1	Analysis type		
0	Cone Calorimeter test	1 - true	0 - false
2.4	Height (m)		
0.61	Width (m)		
0.0127	Thickness (m)		
2	Number of nodes in the horizontal direction		
500	Number of nodes in the vertical direction		
0.475	Thermal inertia ($k\rho c$) $(kW/m^2\ K)^2$ sec		
623.0	Ignition temperature (T_{ig}) (K)		
15000.0	Heat of combustion (kJ/kg)		
0.64	Percent of the mass burned of (1- this is what remains)		
473.0	Density (kg/m^3)		
700.0	Pyrolysis temperature (K)		
305.0	Ambient temperature (K)		
433.0	Initial Temperature (K)		
2	Fire type (Flame height correlation)		
5.2	Imposed flux (kW/m^2)		
37.0	Flame flux after ignition (kW/m^2)		
1.0	Temperature difference (°C or K)		
6	Flame heat flux correlation		
0.0	Used only with flame heat flux correlation # 4		
0	0 - do not use special line fire fluxes, 1, 2 - use forms		
0	Convection factor (W/m^2-K)		
0.5	Emissivity/Absorptivity of the material surface		
1.08	This is the minimum ratio between the fire height and the pyrolysis height		
300.0	Time max (sec)		
1.0	Calculation interval (sec)		
0.25	HRR/unit length (kW/m)		
15.0	Time to burner to rise (sec)		
0	Number of voids		

A - 4 Input data: Full-scale Wood Particle Board

7	Version control flag (current version requires a 1 to run)		
0	Burner control flag	0 - normal	1 - never shut off
0	Debug on		
1	Analysis type		
0	Cone Calorimeter test	1 - true	0 - false
1.8	Height (m)		
0.30	Width (m)		
0.013	Thickness (m)		
2	Number of nodes in the horizontal direction		
500	Number of nodes in the vertical direction		
0.475	Thermal inertia ($k\rho c$) $(kW/m^2\ K)^2$ sec		
623.0	Ignition temperature (T_{ig}) (K)		
14000.0	Heat of combustion (kJ/kg)		
0.65	Percent of the mass burned of (1- this is what remains)		
600.0	Density (kg/m^3)		
700.0	Pyrolysis temperature (K)		
298.0	Ambient temperature (K)		
298.0	Initial Temperature (K)		
5	Fire type (Flame height correlation)		
0.0	Imposed flux (kW/m^2)		
30.0	Flame flux after ignition (kW/m^2)		
1.0	Temperature difference (°C or K)		
1	Flame heat flux correlation		
0.0	Used only with flame heat flux correlation # 4		
0	0 - do not use special line fire fluxes, 1, 2 - use forms		
0	Convection factor (W/m^2-K)		
0.9	Emissivity/Absorptivity of the material surface		
0.0	This is the minimum ratio between the fire height and the pyrolysis height		
3000.0	Time max (sec)		
1.0	Calculation interval (sec)		
22.0	HRR/unit length (kW/m)		
20.0	Time to burner to rise (sec)		
0	Number of voids		